THE FORMATION OF SUBSTELLAR COMPANIONS DUE TO PROTOSTELLAR DISK INSTABILITIES: MODELING THE EFFECTS OF THE GRAVITATIONAL ENVIRONMENT

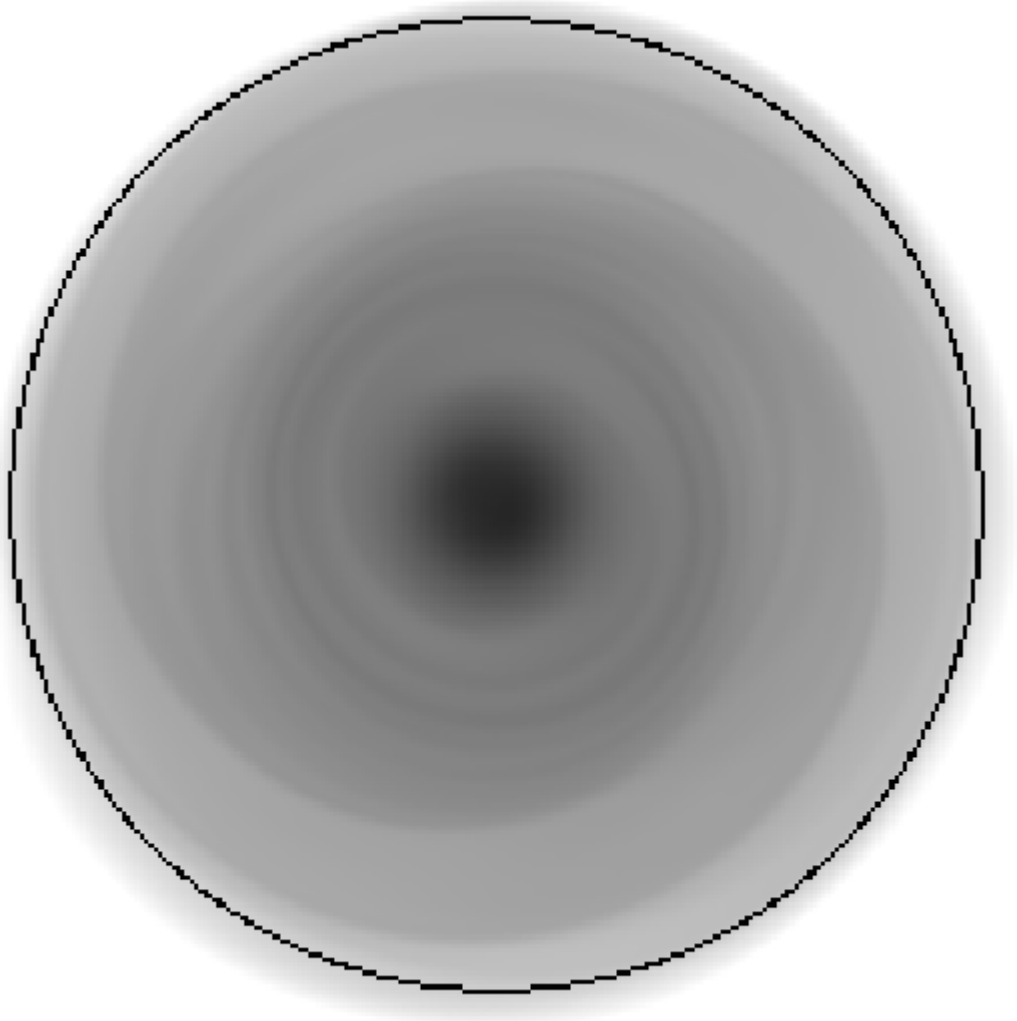

Kathy Cooksey
Valparaiso University

THE FORMATION OF SUBSTELLAR COMPANIONS DUE TO PROTOSTELLAR DISK INSTABILITIES: MODELING THE EFFECTS OF THE GRAVITATIONAL ENVIRONMENT

Kathy Cooksey
Valparaiso University

Advisor: Dr. Brian K. Pickett
University of Purdue Calumet

Committee: Dr. Bruce Hrivnak, Dr. Donald Koetke,
Department of Physics and Astronomy;
Dr. Ken Luther, Department of Mathematics,
Valparaiso University

Submitted to the College of Arts and Sciences
in partial fulfillment of the requirements
for the degree
Bachelor of Science with Honors in Physics
in the Department of Physics and Astronomy,
Valparaiso University, Indiana
May 2003

Honor Code: I have neither given or received nor have I tolerated others' use of unauthorized aid.

ACKNOWLEDGEMENTS

I am very grateful to my advisor Dr. Brian K. Pickett for his support and guidance during my college career and especially during this project. I would also like to thank my honors thesis committee: Dr. Bruce Hrivnak, Dr. Donald Koetke, and Dr. Ken Luther. This work was supported by the College of Arts and Sciences and the Department of Physics and Astronomy of Valparaiso University, Indiana.

Last but not least, I must thank my fellow physics major and best friend, Nicolas George. Without him, I would not be the person I am today.

ABSTRACT

Modern observations have shown that the majority of stars are found in binary or even multiple star systems and that these systems form during the early stages of the stellar evolution. In addition, the number of stars with known planetary companions has increased dramatically in recent years. However, the process of stellar and substellar companion formation is not well understood. This study builds upon the work of Pickett et al., who have simulated the evolution of environmentally isolated, self-gravitating, rapidly rotating protostellar disks in order to characterize the conditions under which substellar companions form in condensations of gas and dust. Using a modified version of their three-dimensional hydrodynamics code, this study examines the gravitational effects of the surrounding environment on the evolution of a protostellar disk.

CONTENTS

FIGURES and TABLES

1. INTRODUCTION

Observations show that the majority of stars are part of binary or multiple star systems. Indeed, stars appear to form in these systems very early in their evolution (Tohline 2002). In addition, recent advances in technology have allowed for improved detection of extrasolar planets, and over a hundred planets have been discovered to date (Schneider 2003). However, the process of multiple star system formation or planet formation is not well understood. This study builds upon the work of Pickett et al. (2000) and seeks to increase the realism with which the conditions of early stellar evolution are modeled and explore the resulting effects on substellar companion formation.

1.1. Star Formation

Stars form in cold, dense regions comprised mostly of molecular hydrogen and helium called giant molecular clouds (GMCs). In these clouds, denser regions of self-gravitating, slowly rotating material called molecular cloud cores (MCCs) develop, perhaps due to turbulent motions in the GMCs or collapsing magnetic fields (Tohline 2002). Eventually, an MCC becomes dense enough to begin gravitational collapse. As the core contracts to stellar density, it rotates faster and forms an extended, rapidly rotating disk of gas and dust at its equator. Material from the enshrouding molecular cloud continues to accrete onto the core, now called a protostar. As the embedded protostar evolves towards the main sequence, it develops a stellar wind, which escapes along the axis of rotation where the density of material is least. The disk transports angular momentum away from the protostar, and material with high angular momentum begins accreting preferentially onto the protostellar disk. This allows the opening angle of the stellar winds to increase, which eventually clears away the surrounding region of the molecular cloud. At this point, the now pre-main sequence star and protostellar disk are observable in visible wavelengths.

2. SIMULATION PROCESS

Before the young stellar winds dissipate the protostellar disk, after about 10^6-10^7 years, stellar and substellar companions (e.g., brown dwarfs, giant gaseous protoplanets) may form from the condensation of the remaining gas and dust in the disk. It is this brief phase in the stellar lifetime that is the focus of this study.

2.1. 3-D Hydrodynamics Code: Pickett et al. (1998, 2000)

Previously, Pickett et al. have simulated the evolution of environmentally isolated, self-gravitating, rapidly rotating protostellar disks in the linear regime with their fully three-dimensional hydrodynamics code. The code creates a three-dimensional disk by loading a two-dimensional axisymmetric model in equilibrium onto a three-dimensional cylindrical grid with equatorial plane symmetry and resolution (r, φ, z), such as (128, 128, 16). The model is initially in thermal, gravitational, and rotational force balance. The disk may be artificially heated or cooled to affect possible physical conditions of the protostellar environment and may be given an initial random density perturbation to stimulate the growth of nonaxisymmetric structure in an unbiased manner. The 3-D hydrodynamics code numerically calculates the accelerations and the movement of material to second order accuracy in space and time on a cylindrical grid, using the Poisson equation and the equations of hydrodynamics, namely, the mass continuity equation, the equations of motion, and an internal energy equation (Pickett 1995). At every hydrodynamics step, a Fourier transform in φ of the density in the equatorial plane gives the Fourier amplitudes a_m and phase angles b_m as a function of time t and cylindrical radius j:

$$a_m(j,t) = \frac{2}{\pi}\sum_{l=1}^{l_{MAX}} \rho(j,\varphi_l,t)\cos(ml\delta\varphi)\delta\varphi \tag{1}$$

$$b_m(j,t) = \frac{2}{\pi}\sum_{l=1}^{l_{MAX}} \rho(j,\varphi_l,t)\sin(ml\delta\varphi)\delta\varphi \tag{2}$$

where the azimuthal grid spacing is $\delta\varphi = 2\pi/l_{MAX}$, l is the azimuthal grid number, and l_{MAX} is the azimuthal resolution of the grid. The relative amplitudes A_m, which measure the strength of a given disturbance with m-fold azimuthal symmetry (Fig. 1), and phase angles φ_m, which measure the coherence of a disturbance across the disk, are defined as follows:

$$A_m(j,t) = \frac{\left[a_m(j,t)^2 + b_m(j,t)^2\right]^{1/2}}{a_o(j)} \sim \frac{\delta\rho_m}{\rho_o} \tag{3}$$

$$\varphi_m(j,t) = \arctan\left(\frac{-b_m(j,t)}{a_m(j,t)}\right). \tag{4}$$

The approximate equality in equation (3) relates A_m to the difference, $\delta\rho_m$, between a cell's density and the initial density over the initial density, ρ_o, for each possible m-value.

The Fourier coefficients and the density in the equatorial plane are written to file every 300 computational steps for adequate time resolution during analysis. Other information about the disk (e.g., mass, angular momentum distribution) are stored every 2000 steps. Simulations are run until significant mass or angular momentum leaves the

computational grid or the center of the disk moves more than one cell from the center of the grid, signifying that the disk has evolved beyond the capabilities of the code.

After a few rotations, the initially randomly perturbed disk begins to organize into over-dense regions that may be precursors to spiral arms or, eventually, substellar companions. Such disturbances may be seen in equatorial density plots, which are convenient measures of the activity in the disk in the non-linear regime (Fig. 1). However, early in their development, the disturbances are best seen in density perturbation plots of the relative amplitudes (Fig. 1). A disturbance with a well-defined *e*-folding time τ_m and pattern period P_m over a significant portion of the disk is considered a mode (Fig. 2). Essentially, the superposition of the density perturbation plots for all *m*-values yields the equatorial density plot (Fig. 1), much the same way that the sum of terms in a Fourier expansion yields the original function. In most cases, the first four *m*-values contribute most significantly to the total disturbance.

Pickett et al. have developed their code to include most of the thermal energetics expected in the disk (e.g., compressional heating due to shocks). In Pickett et al. (2000), hereafter Paper I, they studied the effect that increasingly realistic internal energy constraints had on the evolution of an environmentally isolated, self-gravitating, rapidly rotating protostellar disk in the linear regime. Here, linear refers both to the small size of the density perturbation, when $A_m < 0.1$, and the exponential growth of the disturbance.

2.2. 3-D Hydrodynamics Code: Gravitational Environment

It is believed that the majority of stars form in clusters of gravitationally bound stars (Lada et al. 1993). Therefore, the next step in making the 3-D hydrodynamics code more realistic is the inclusion of the presumably destabilizing effects of neighboring stars on the evolution of a protostellar disk. Towards this end, a supplemental program has been developed to generate a star cluster based on the following parameters: number of cluster objects, cluster member mass range, cluster radius, and disk radius and mass (see Appendix A). First, the program assigns each cluster member a random location (*x*, *y*, *z*) in the Cartesian coordinate system so that the distance from the origin is equal to or less than the specified cluster radius (Fig. 3); this assumes that the cluster members are randomly distributed in space, as is seen in young clusters (Lada et al. 1993). The program next uses the Monte Carlo method to assign each member a mass. Observations show that there are generally more low mass stars than high mass ones, and the initial mass function (IMF) for low mass stars is a probability distribution that describes this trend:

$$P(M_{OBJ}) = \left(\frac{M_{OBJ}}{M_{MIN}} \right)^{-1.5}, \qquad (5)$$

where M_{OBJ} is the mass of the cluster member and the minimum object mass, M_{MIN}, normalizes the function (Fig. 4; Lada et al. 1993). The program saves the locations and masses of the specified number of cluster members to a file for use in the 3-D hydrodynamics code and other analysis.

The clusters generated by this program showed no obvious bias in the locations assigned by the random number generator. To demonstrate this more quantitatively, the spatial distributions were subjected to a more rigorous test of randomness (Fig. 5). Linear regressions were performed individually on the *x*, *y*, and *z* positions as a function

of the cluster member, which was assigned a number in the order that it was generated. If a distribution were truly random, the slope of the linear regression for a large data set would be zero. The x and y distributions were within a half standard deviation of zero, and the z distribution was within two standard deviations for the generated clusters used in this study.

The 3-D hydrodynamics code has been modified to import the masses and positions of the cluster members (see Appendix B). The code calculates the gravitational potential $\Phi_{G,i}$ due to each member of mass M_i a distance d_i from the center of each cell (j, l, k) in (r, φ, z) of the computational grid:

$$\Phi_{G,i}(j,l,k) = -\frac{M_i}{d_i(j,l,k)} \tag{6}$$

(Fig. 6). The grid itself can be placed at any location with respect to the Cartesian coordinate system discussed previously. For each computational cycle, the code updates the total internal gravitational potential Φ_{INT} for each cell and adds the perturbation $\Phi_{G,i}$ of the N cluster members to obtain the total potential Φ_{TOT}:

$$\Phi_{TOT}(j,l,k) = \Phi_{INT}(j,l,k) + \sum_{i=1}^{N} \Phi_{G,i}(j,l,k). \tag{7}$$

To test that the modifications of the code worked as expected, a point source of comparable mass located within a few protostar radii was included in a test simulation of a well-understood protostar model known to develop a dominant, global $m = 2$ mode in simulations without the gravitational influence of a star cluster. Very rapidly, the model moved off the computational grid as expected for such extreme conditions.

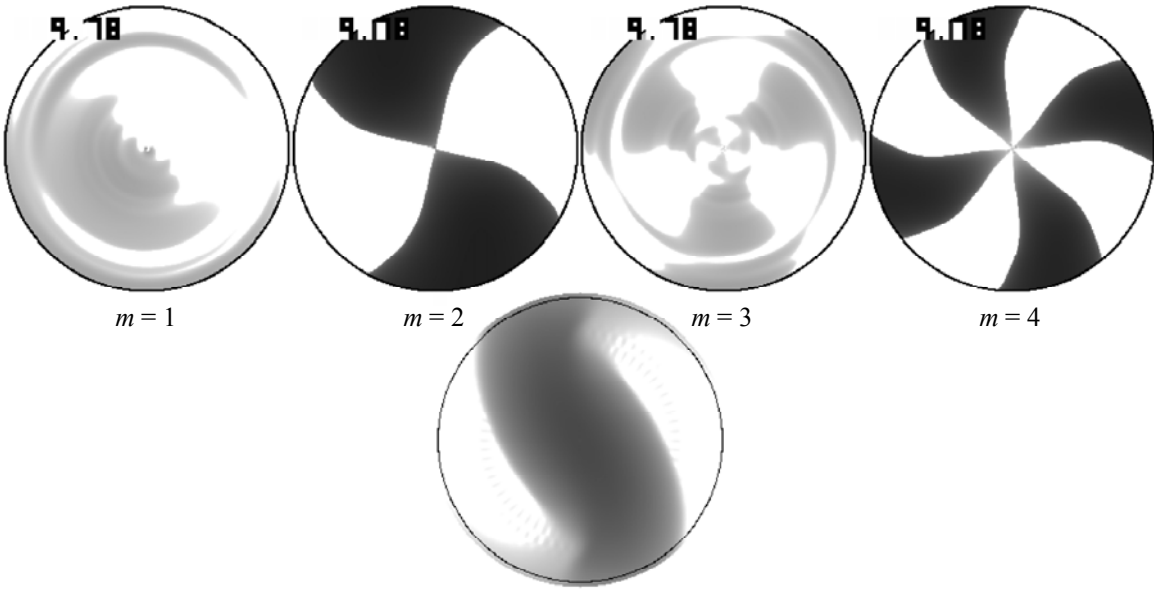

Figure 1: Essentially, the superposition of the density perturbation plots for all m-values forms the equatorial density plots. Generally, the m = 1-4 components are the most important. The evolution of a well-studied protostar model (Pickett 1995) was dominated by a global m = 2 mode, as seen in the equatorial density plot where black is for $\rho = 0.3$ and white for $\rho = 3\text{x}10^{-7}$ (*bottom*). The density perturbation (*top*) show the very coherent over-density of material in the disk due to the m = 2 component of the disturbance; the m = 4 component has some elements of the m = 2 component and is also coherent. The scale for the density perturbation plots is black for $\log(A_m) = 0$ and white for $\log(A_m) = -5$. For all images, the time is 9.78 central initial rotation periods (CIRPs, see Appendix C), the black outline indicates the initial size of the model, and the sense of rotation is counter-clockwise.

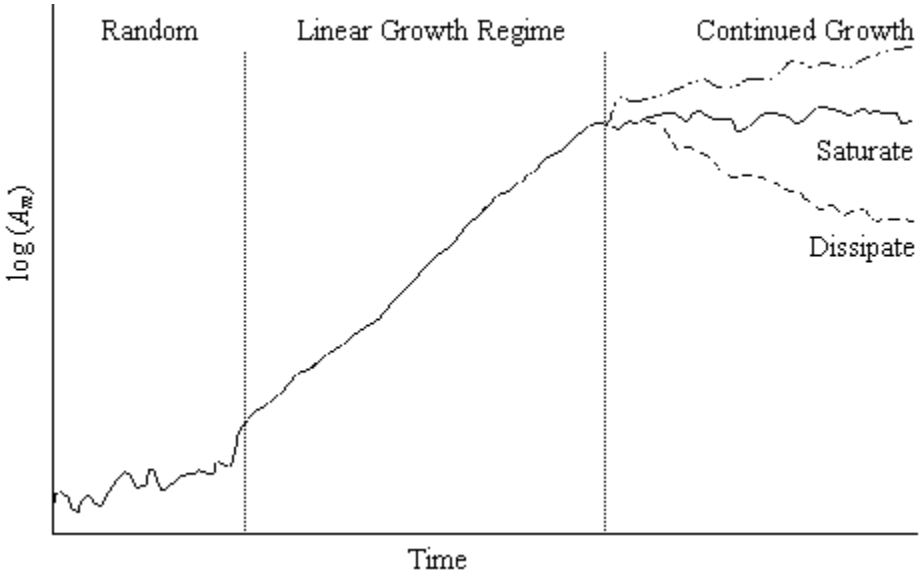

Figure 2: The general evolution of the *m*-component of a disturbance in the disk can be characterized by plotting the time evolution of $\log(A_m)$, as defined by equation (3). Initially, the material in the disk is randomly distributed. Then, a disturbance with *m*-fold symmetry may grow in some portion of the disk. When this growth is exponential, it is called the linear growth regime, and the slope of this portion of the amplitude plot is the *e*-folding time τ_m. The disturbance rotates with a pattern period P_m that may be measurable during the growth regime. The disturbance will either continue to grow, saturate, or dissipate after the linear growth regime. When the disturbance continues to grow, it suggests that the apparent linear growth regime was a rapid burst of activity and growth within a longer growth period, and growth times are measured for both periods. When the disturbance saturates, it persists at its greatest $\log(A_m)$ level for the remainder of the simulation and rotates with a specific P_m. In some cases, the protostellar disk becomes stable to nonaxisymmetric structure, and the disturbance dissipates (i.e., $\log(A_m)$ decreases). Many models evolved with the 3-D hydrodynamics code develop different disturbances, with characteristic τ_m and P_m, in separate regions of the disk.

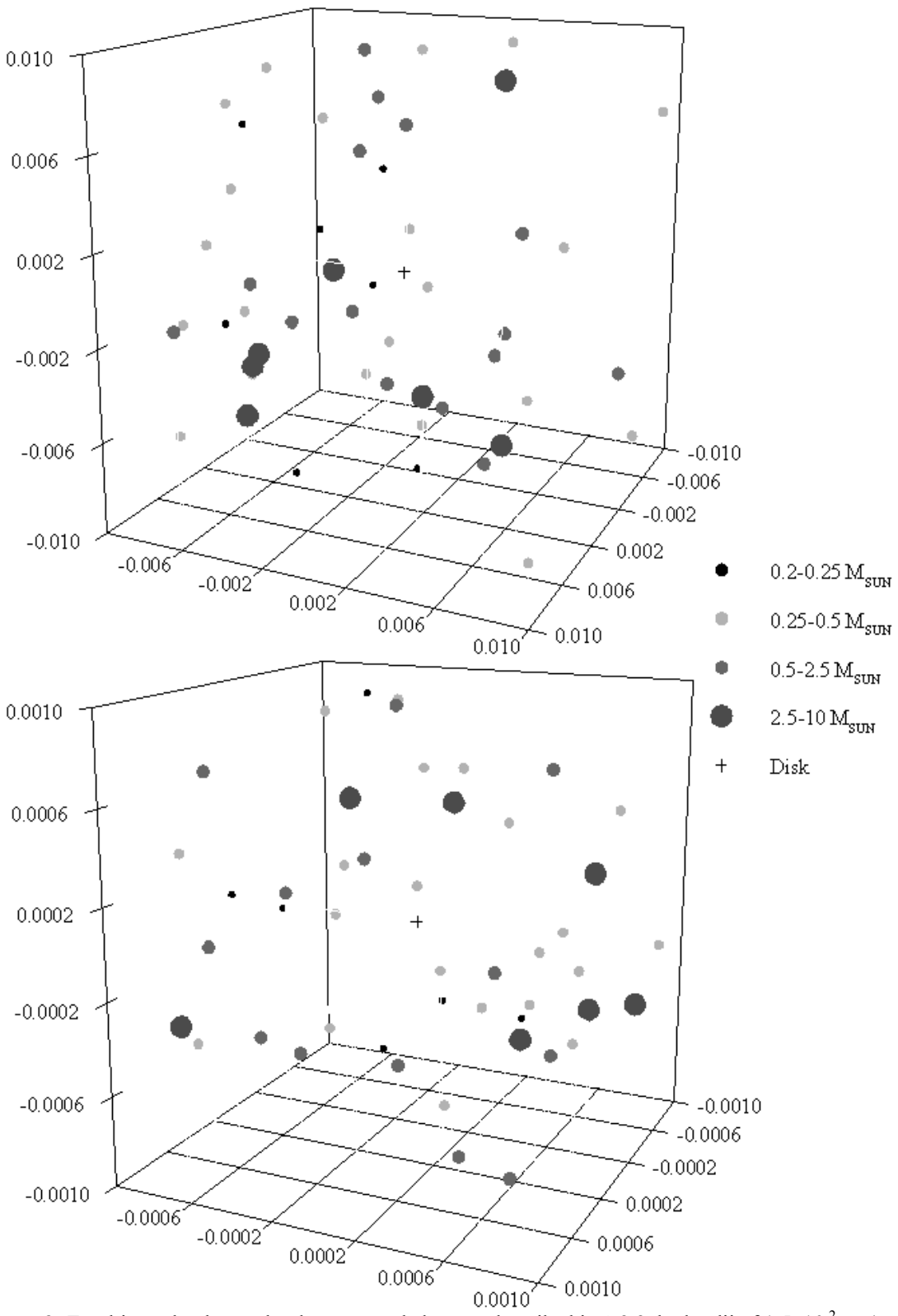

Figure 3: For this study, the randomly generated clusters, described in § 2.2, had radii of 1.5×10^{-2} pc (*top*), 1.5×10^{-3} pc (*bottom*), and 1.5×10^{-4} pc, which was a scaled version of the 1.5×10^{-2} pc cluster. The mass range for the 50 members is 0.2-10 M_{SUN}. The marker sizes indicate the mass range of the objects. The computational grid is approximately at the center of this schematic (cross).

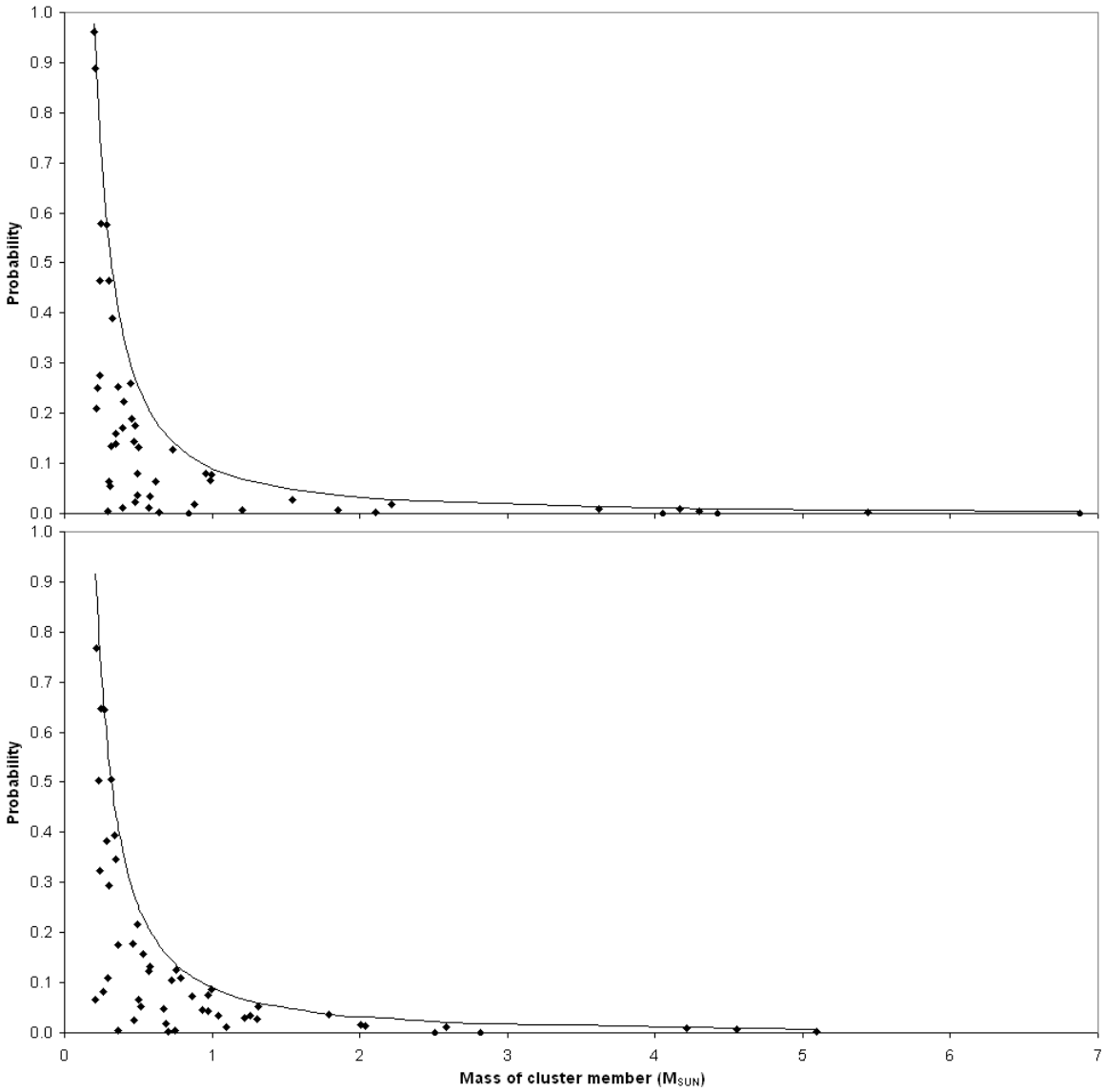

Figure 4: The initial mass function (IMF) for low mass stars, described by equation (5), constrains the mass distribution so that there are more low mass stars than high. The distributions are shown for the 1.5×10^{-2} pc (*top*) and the 1.5×10^{-3} pc clusters (*bottom*). In the program that generates star clusters for the 3-D hydrodynamics code, each member is randomly assigned a mass and probability (points). If this probability is less than or equal to the probability calculated using the assigned mass and IMF (line), the program accepts this mass and records it to file. Otherwise, the mass is discarded, and the process repeats until every cluster member has been assigned a mass obeying the IMF.

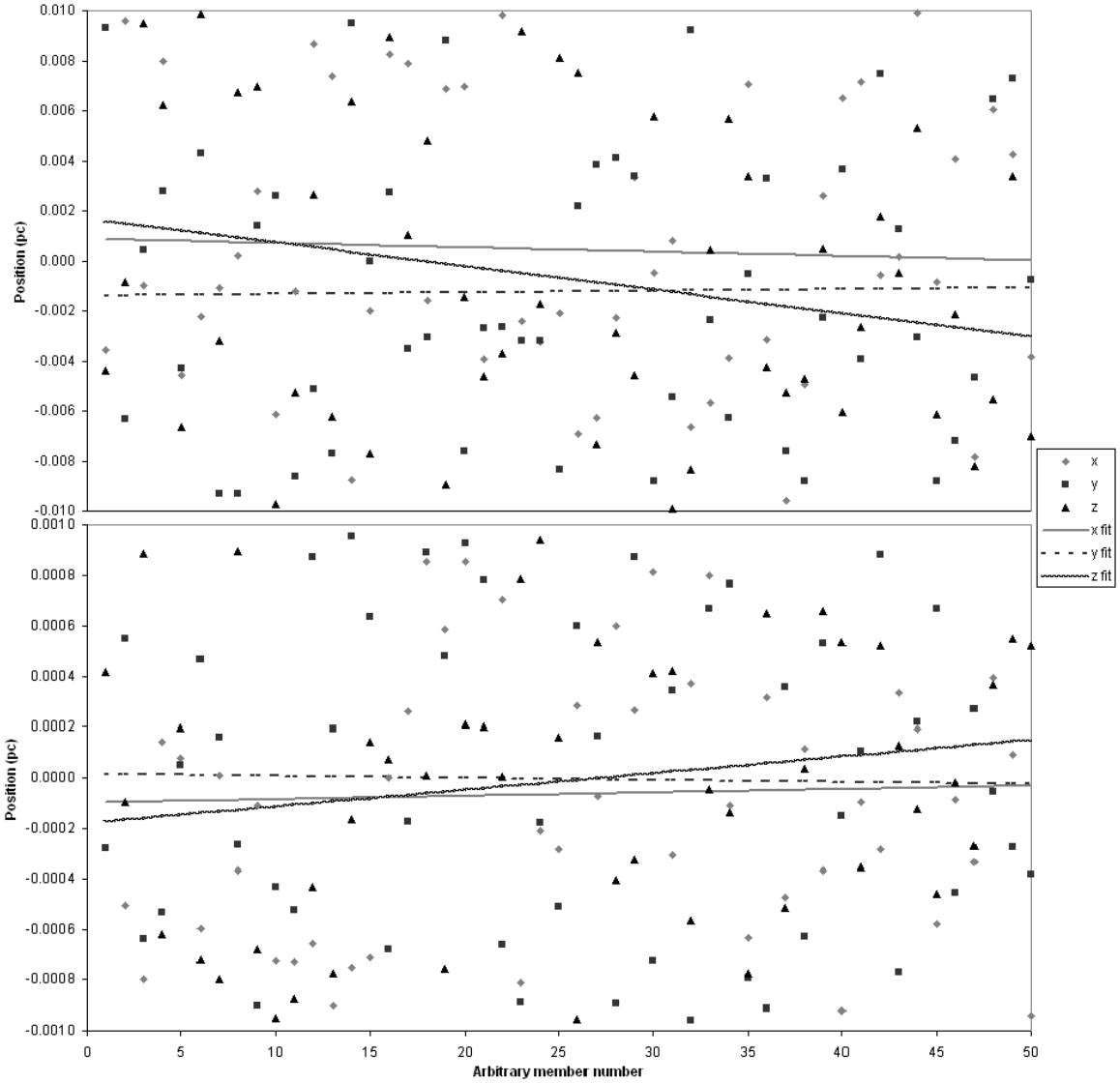

Figure 5: The *x*, *y*, and *z* positions were plotted as a function of the cluster member, which was assigned a number in the order that it was generated, for the 1.5×10^{-2} pc (*top*) and 1.5×10^{-3} pc clusters (*bottom*). Linear regressions were performed on each distribution as a quantitative test of the randomness of the cluster-generating program. For both clusters, the *x* and *y* distributions were within a half standard deviation, and the *z* distributions were within two standard deviations.

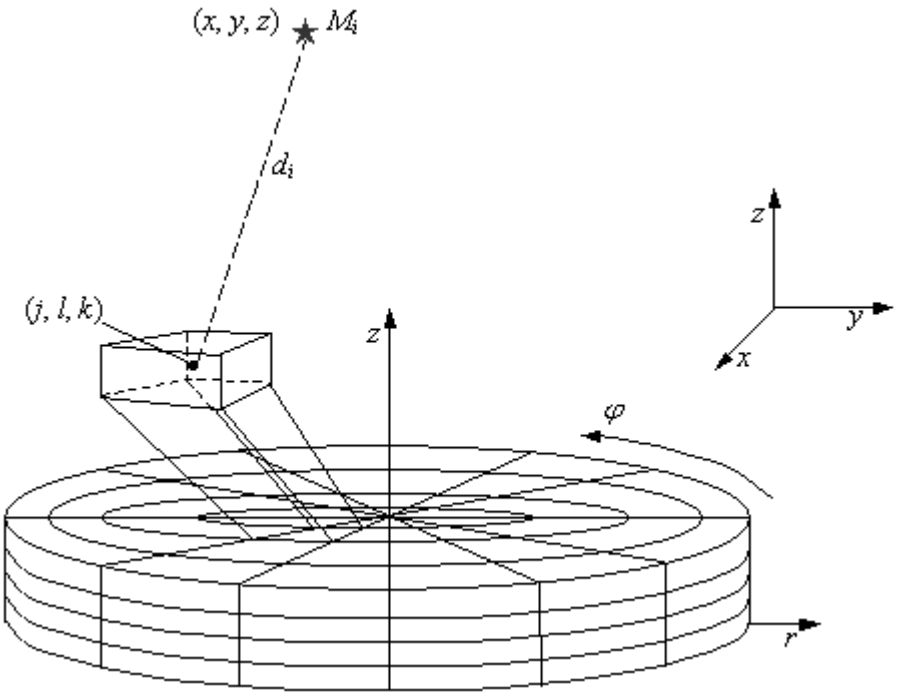

Figure 6: The protostellar disk model is centered on a cylindrical grid with resolution (r, φ, z), and the center of each cell has coordinates (j, l, k) in this coordinate system. The star cluster is centered on a Cartesian coordinate system, which may or may not correspond to the disk center. Each cluster member is a point source of mass M_i with location (x, y, z). To calculate the gravitational perturbation as defined by equation (6), the 3-D hydrodynamics code transforms the star's location into grid coordinates and calculates d_i, the distance between the star and the cell center.

2.3. Protostellar Disk Model

The current paper focuses on the protostellar disk model thoroughly studied under progressively more energetically realistic simulations in Paper I. The local temperature was held fixed at its initial axisymmetric distribution in the locally isothermal case (ISO). As a better thermal approximation, the entropy remained similarly fixed for the locally isentropic case (ISE). These cases allowed significant thermal energy to be lost through radial motion during the course of the evolution. Pickett et al. also incorporated an internal energy equation into the hydrodynamics code to account for heat loss at the shock fronts of material moving azimuthally. The internal energy equation conserved entropy and permitted heating and cooling. For the adiabatic case (ADI), both the heating and cooling terms were set to zero, rendering irreversible compression unimportant. Finally, artificial viscosity approximated the heating due to shock fronts in the adiabatic with artificial viscosity case (ADI + AV); no cooling term was used. In Paper I, Pickett et al. discovered that the dominant $m = 2$ mode in the ISO simulation became less coherent and strong through the ISE and ADI simulations. Ultimately, shock heating in the ADI + AV simulation stabilized the disk, and little nonaxisymmetric structure developed (Fig. 7).

The gravitational influence of a star cluster was incorporated in addition to the thermal conditions of the ADI + AV case for the same protostellar model in all simulations of the current study. The protostellar disk model studied here, as in Paper I, has a mass equal to 0.5 M_{SUN} and a radius of 0.1 AU. Most protostellar disks are several solar masses and ~10-10^3 AU across (Tohline 2002). Star clusters in star forming regions are ~10^{-1} pc in diameter with ten to a hundred members (Lada et al. 1993). Since the disk model is smaller than average, three simulations were run with cluster radii of 1.5×10^{-2} pc, 1.5×10^{-3} pc, and 1.5×10^{-4} pc and 50 cluster members of masses between 0.2-10 M_{SUN} (Fig. 3). The two simulations with the larger cluster radii ran for over 33 minimum initial rotation periods (MIRPs), which was the time presented in Paper I. Here, a MIRP is the orbital period of material at the inner edge of the disk, at the star-disk boundary, and represents the fastest orbital motion. In the simulation with the smallest cluster radius, the gravitational perturbation was too great and pulled the model from the computational grid in less than 7 MIRPs. All simulations were given a small random initial perturbation with magnitude $\delta\rho/\rho_o \leq 0.005$ in the region $0.5 \leq j/R_{eq} \leq 1.0$, as done in all cases of Paper I. R_{eq} is the initial equatorial radius of the model; the units used in this paper are discussed in Appendix C.

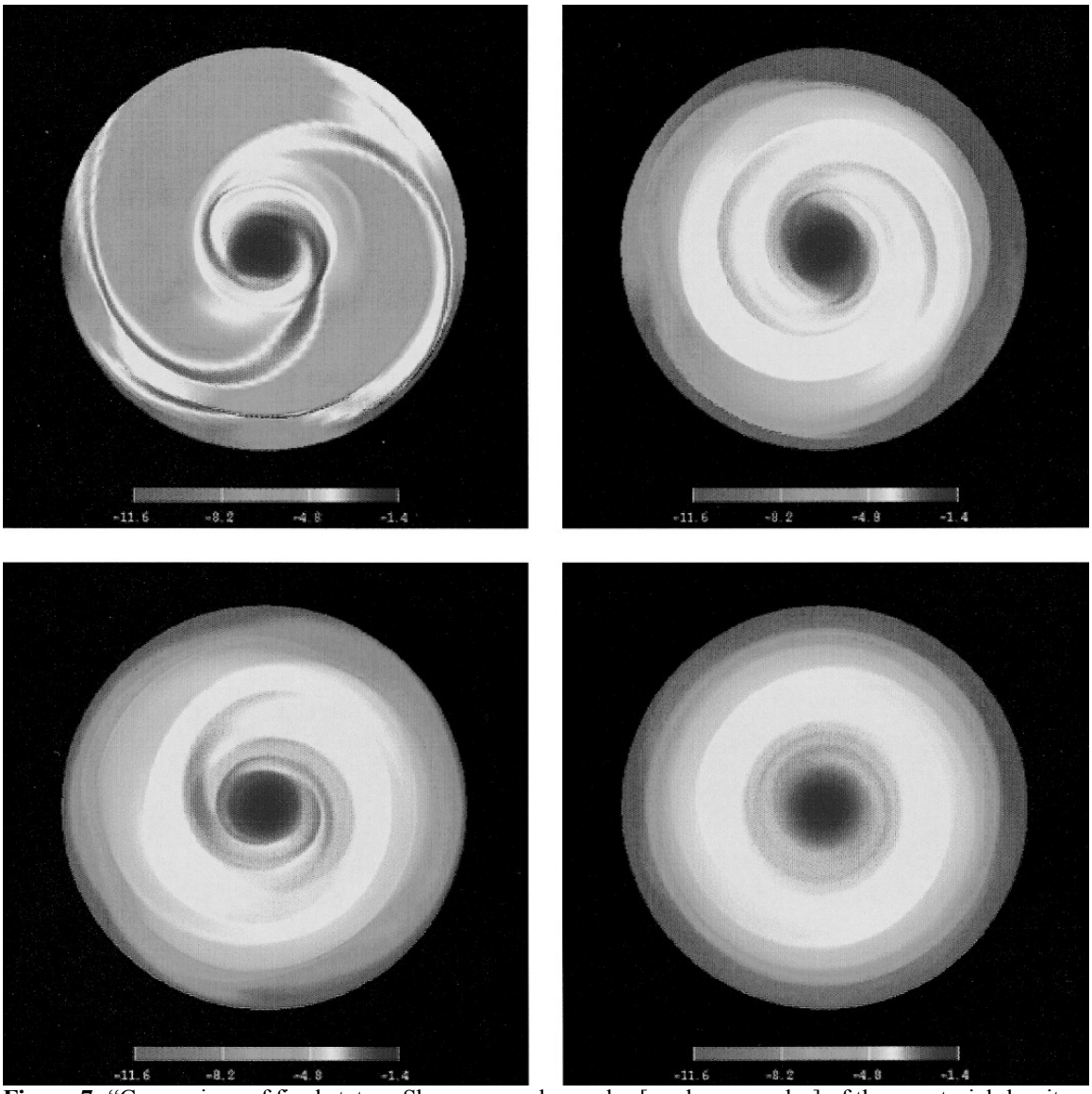

Figure 7: "Comparison of final states. Shown are color scales [made grayscales] of the equatorial density at the end of the four main simulations using (128, 64, 16) resolution discussed here and in Paper I [Pickett et al. 1998]. The images are from the locally isothermal case at t = 20.0 minimum initial rotation periods, or MIRPs (*top left*), the ADI case at t = 38.0 MIRPs (*top right)*, the locally isentropic case at t = 33.0 MIRPs (*bottom left*), and the ADI + AV case at t = 33.0 MIRPs (*bottom right*)" (Fig. 11, Paper I; reproduced from *Astrophysical Journal*).

3. ANALYSIS and RESULTS

3.1. Procedure

To compare quantitatively the change that the gravitational environment induced on the previously marginally stable protostellar disk, the *e*-folding times τ_m and pattern periods P_m of the m = 2-4 components of the disturbance were determined for the simulations with 1.5×10^{-2} pc and 1.5×10^{-3} pc clusters. As mentioned previously, the simulation with the 1.5×10^{-4} pc cluster evolved very rapidly and violently, and no quantitative analysis could be performed.

To view the general evolution of the disk, the log of the relative density, $\log(A_m)$, of each radius was plotted over time (Fig. 8). This three-dimensional Fourier amplitude surface is made two-dimensional by adjusting the perspective at each radial position. The original analysis code of Paper I that generates the Fourier amplitude surface was only capable of plotting 20 MIRPs. To fit the full 33 MIRPs of the simulations with the star clusters, the MIRP was scaled by a factor of 7/4. The growth times and errors were later adjusted by the same factor to obtain the appropriate value in MIRPs (see Appendix C). The Fourier amplitude surface allowed for an intuitive understanding of which region of the disk underwent a linear growth to saturation and whether the component later dissipated.

The slopes of the linear growth regime at each radius were measured by a least squares fit of the relative amplitude (Fig. 9). Again, the analysis code of Paper I was used, and the MIRP was scaled, as discussed previously. On occasion, there was a brief, short linear growth but also an overall trend of continuous growth; both were fitted (Fig. 2). Short, steep linear growth regimes led to larger errors compared to the growth times. The saturation level relates to the strength of the *m*-value component. For instance, the m = 2 component in Figure 9 saturated at ~18%, whereas the m = 3 saturated around ~6% (see Table 1). Recall that an $A_m \sim \delta\rho_m/\rho_o$, and so A_3 ~6% means that a three-armed disturbance has created an over-density of about 6% of the initial value. Once the growth times of the individual radii were measured and compiled, they were examined for regions in which the *m*-value grew in about the same time during the simulation with approximately the same growth time. These values and their root mean square errors were averaged and corrected by the 7/4 scale factor to obtain the growth times and errors (see Appendix C). The values quoted in Table 1 are for the *m*-components of the disturbance that grew with the same τ_m and rotated with a distinct P_m in the same radial range.

In the simulations presented here and in Paper I, the protostellar disk model included the central protostar and a continuous star-disk boundary at 0.15 R_{eq}. The protostar developed disturbances with growth times and pattern periods. Because the focus of this study was the formation of substellar companions through disk instabilities, only the disk region of the model was thoroughly analyzed for developing disturbances.

The pattern periods were determined by the auto-correlation function, which performs a sinusoidal least squares fit to the Fourier phase angle φ_m, and the periodogram, which is a "time series analysis tool that produces power spectra for each radius" (Pickett 1995). When a simulation evolves cleanly and with a dominant mode, the pattern period can be measured during the linear growth regime. For the simulation presented here, the evolution of the disk was more complicated, and the pattern periods

were fit to the time for which the *m*-value remained at its saturation level. It was not necessary to correct the pattern periods with the scale factor.

The auto-correlation function plots the time-varying $\cos(\varphi_m)$, in a manner similar to the plot of the Fourier amplitude surface, for the radial range of interest (*top*, Fig. 10). This permitted a visual verification of the coherence of the *m*-component. The pattern period was measured by fitting a sinusoid to the combined $\cos(\varphi_m)$ (*bottom*, Fig. 10). These values and errors are presented (Table 1). The periodogram used a Fourier transform of the phase angles to create power spectrum of the frequency for each radius of the disk (*top*, Fig. 11). The pattern period was measured by finding the peak in the combined power spectrum (*bottom*, Fig. 11).

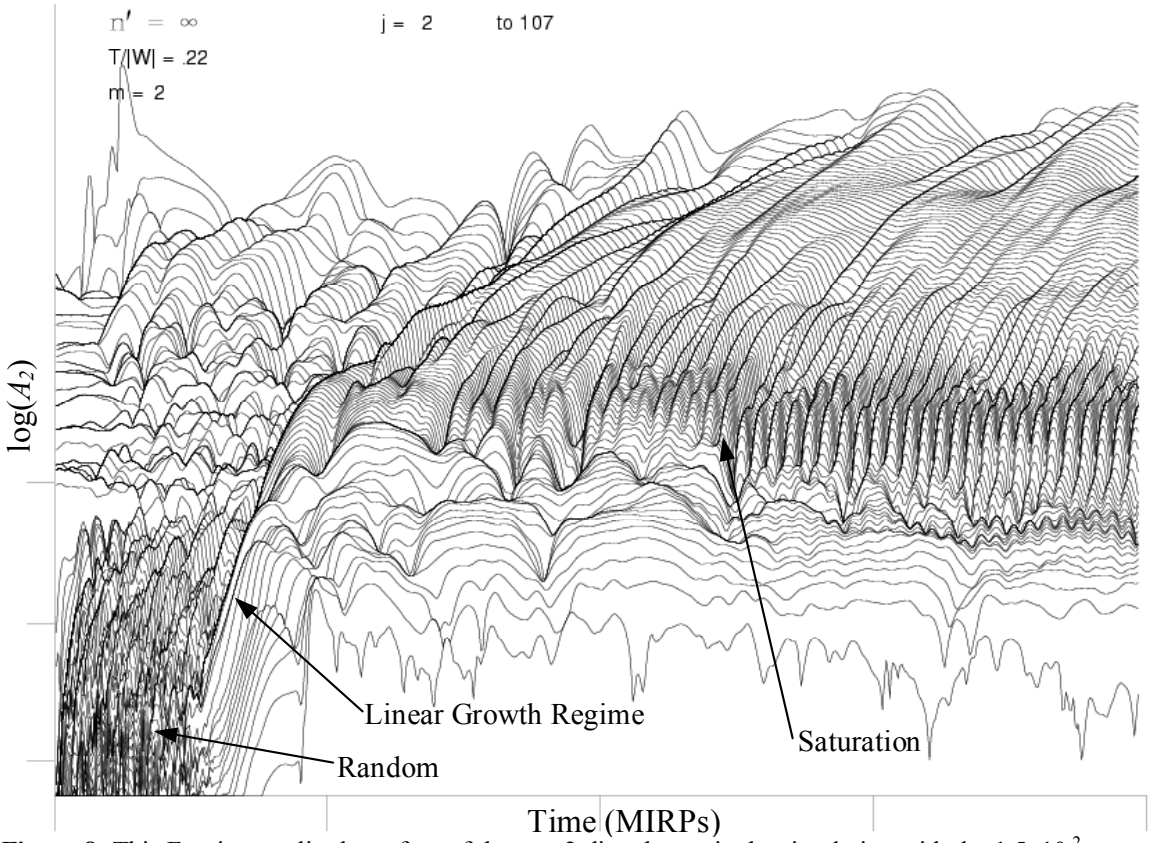

Figure 8: This Fourier amplitude surface of the $m = 2$ disturbance in the simulation with the 1.5×10^{-2} pc cluster gives a general overview of the evolution of all parts of the disk. Each line traces $\log(A_2)$ at a specific radius for the 33 MIRPs of the simulation; the perspective has been adjusted at each radius j to make this three-dimensional plot align properly on the two-dimensional axis. The regions of initial random distribution, linear growth, and saturation as described in Figure 2 are generally indicated.

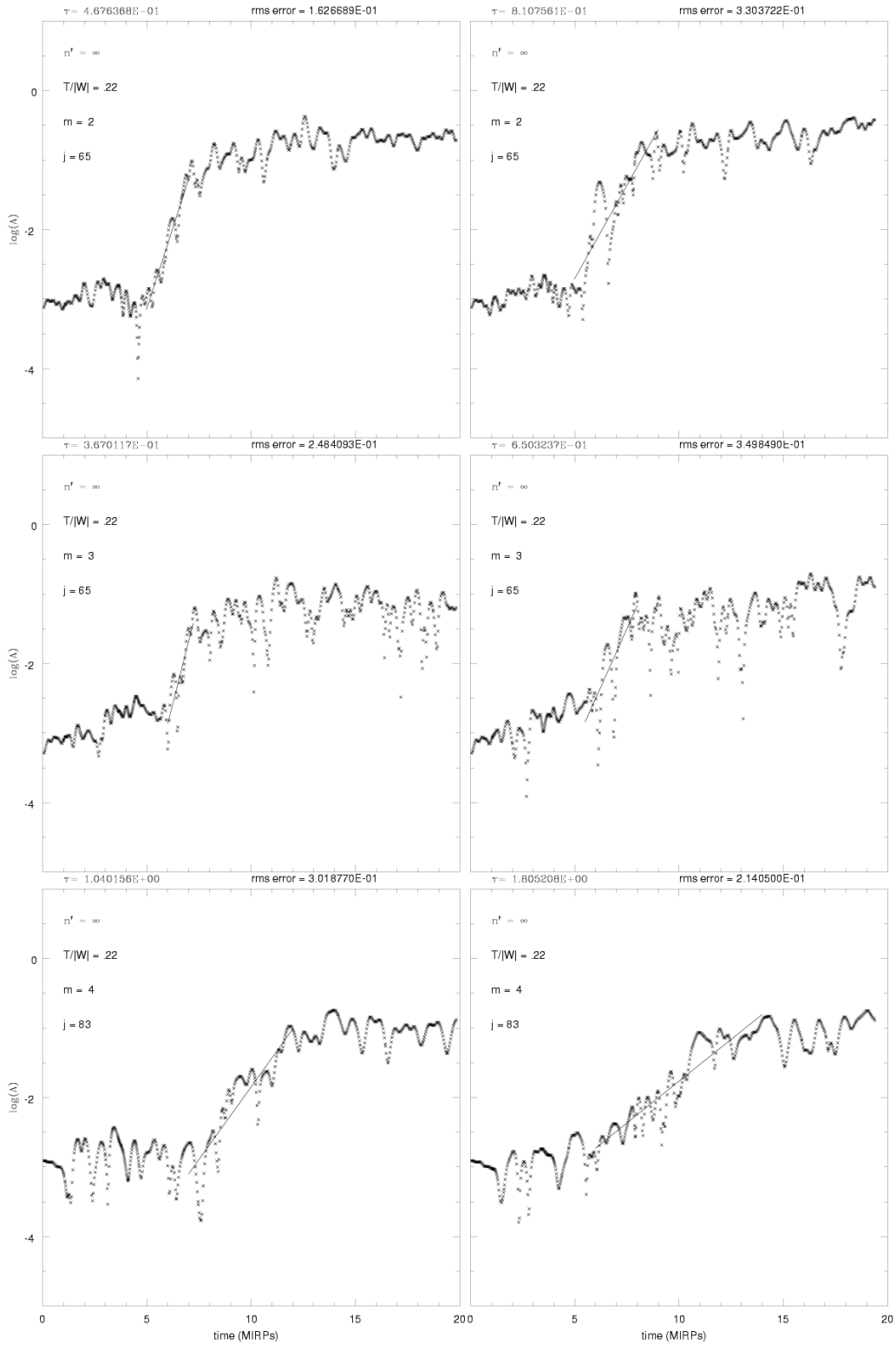

Figure 9: The *e*-folding time and error at incremental radii *j* were measured by a least squares fit to the linear growth regime for m = 2-4. The growth times quoted in Table 1 are the averaged and scaled values (see § 3.1) over the radial range in which an *m*-component of the disturbance grew in approximately the same τ_m during the simulation with a distinct pattern period. These images show the fits in about the middle of the radial range of the simulations with the 1.5×10^{-2} pc (*left*) and 1.5×10^{-3} pc clusters (*right*) for the *m*-value indicated.

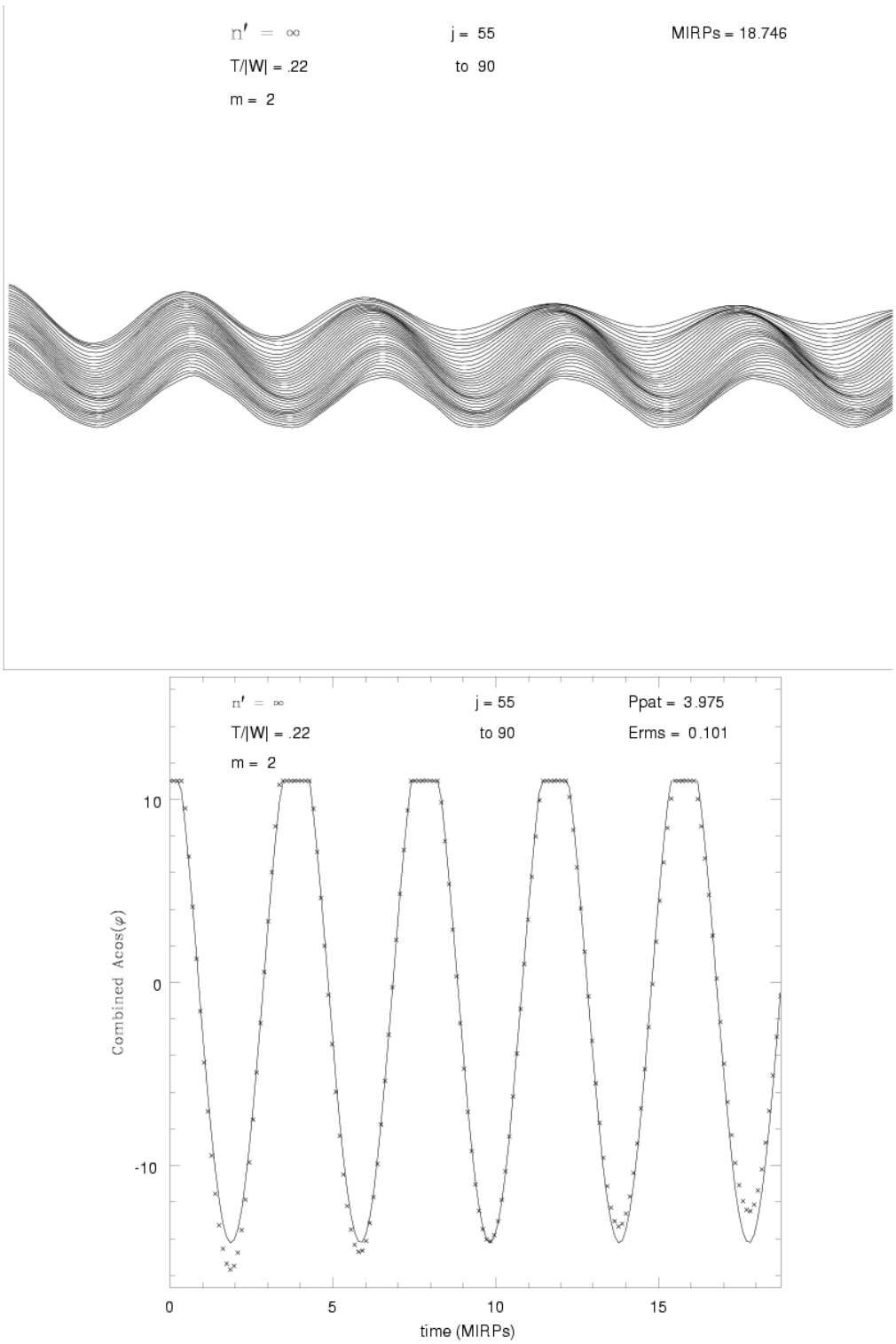

Figure 10: To find the pattern period, the auto-correlation function plots the time evolution of cos(φ_m), times some amplitude, for the radial range with the common growth time (*top*). As in the Fourier amplitude surface, the perspective has been adjusted at each radius *j* (Fig. 8). The radial range may be adjusted to focus on the largest region that is most coherent for the length of the simulation. The pattern period P_m (AC) and range quoted in Table 1 is from the sinusoidal least squares fit to the combined cos(φ_m) (*bottom*). These images are for $m = 2$ for the simulation with the 1.5×10^{-2} pc cluster. The peaks of the combined cosine function appear flat in order to display the information at the top of the figure.

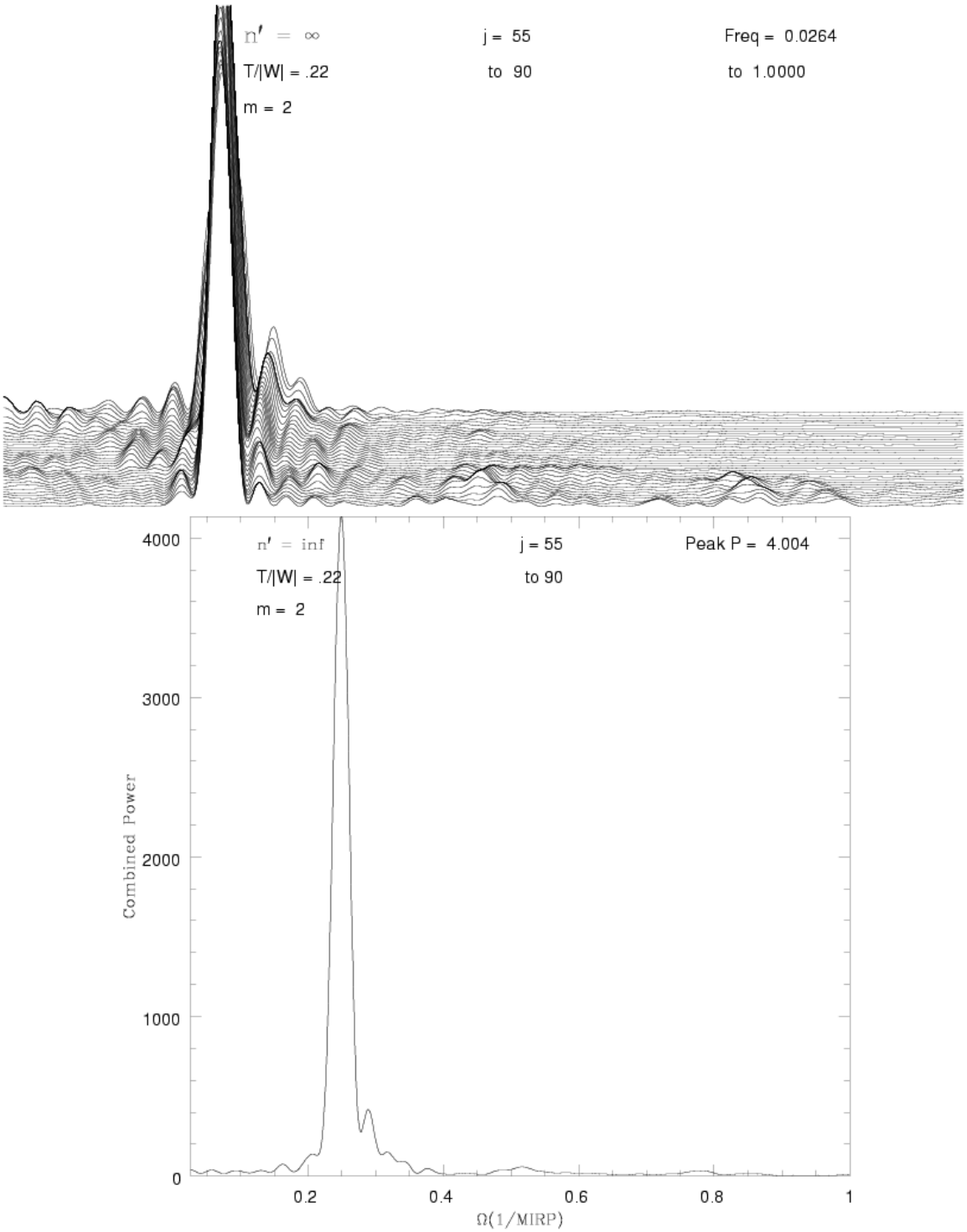

Figure 11: In a process similar to that used with the auto-correlation function (Fig. 10), the periodogram produces a power spectrum of the frequency for each radius *j* in the radial range with a common growth time (*top*). The peak frequency of the combined power spectrum leads to the pattern period P_m (P) listed in Table 1 (*bottom*). These images are for $m = 2$ for the simulation with the 1.5×10^{-2} pc cluster.

Property (r, φ, z)	1.5×10^{-2} pc Cluster (128, 128, 16)	1.5×10^{-3} pc Cluster (128, 128, 16)	ADI + AV (128, 64, 16)	ISO (128, 64, 16)
		m = 2		
τ_2 …	1.04 ± 0.35	1.12 ± 0.52	3.0	2.4
Range …	0.51-0.84	0.47-0.66	0.30-0.62	0.26-0.59
P_2 (AC)…	3.98 ± 0.10	4.099 ± 0.048	3.6	3.5
P_2 (P)…	4.00	4.13	—	—
Saturation …	18%	18%	16%	100%
		m = 3		
τ_3 …	1.94 ± 0.38	1.68 ± 0.42	0.99	1.2
Range …	0.52-0.83	0.47-0.69	0.04-0.26	0.06-0.15
P_3 (AC)…	3.76 ± 0.29	4.18 ± 0.21	0.99	1.0
P_3 (P)…	3.99	4.22	—	—
Saturation …	6%	6%	13% → 1%	10%
		m = 4		
τ_4 …	2.56 ± 0.48	2.99 ± 0.41	0.66	0.75
Range …	0.69-0.85	0.66-0.86	0.04-0.20	0.03-0.26
P_4 (AC)…	3.90 ± 0.19	4.07 ± 0.20	1.0	1.0
P_4 (P)…	3.95	4.08	—	—
Saturation …	10%	10%	10% → 1%	32%

Table 1: The e-folding times τ_m (MIRPs), radial range (R_{eq}), and pattern periods P_m (MIRPs) as determined by the auto-correlation function (AC) and the periodogram (P) for m = 2-4 for the simulations run with different cluster sizes are listed. Similar data for the ADI + AV and ISO cases are reproduced from Paper I; the pattern periods were determined from either the auto-correlation function or the periodogram. For this study, the saturation levels of A_m and their stability (e.g., 10% → 1% denotes decrease) have been approximated from Figure 9 and Figures 2 and 7 of Paper I.

3.2. Results and Simulation Comparison

The gravitational influence of the 1.5×10^{-2} pc and 1.5×10^{-3} pc clusters changed the evolution of the protostellar disk model enough so that it developed some persistent nonaxisymmetric structure (Fig. 12). Table 1 presents the results from the two simulations of the current study and the ADI + AV and ISO cases of Paper I. Though the simulations incorporating the gravitational influence of a star cluster also included the same thermal conditions as used in the ADI + AV case, the term ADI + AV case will only refer to the simulation studied in Paper I. For all simulations, the $m = 1$ component of the disturbance did not lead to a coherent growth over a significant portion of the disk and has not been included in this discussion. In Paper I, Pickett et al. used either the auto-correlation function or the periodogram to measure the pattern periods for $m = 2$-4. For $m = 3$-4, Paper I presented the results for within the central region of the protostellar disk model, which has its initial star-disk boundary at 0.15 R_{eq}. Because this study focused on the disturbances in the disk, there can be no quantitative comparison between the results of simulations with star clusters and the cases from Paper I for $m = 3$-4. However, it should be noted that the previous ADI + AV case produced no $m = 3$-4 components in the disk, whereas the present cases do.

Overall, the simulation with the 1.5×10^{-3} pc cluster developed more nonaxisymmetric structure than that with the 1.5×10^{-2} pc cluster (Fig. 12). The $m = 2$ component of the disturbance dominated in both simulations that included the star clusters, as seen by the coherence and strength of the $m = 2$ density perturbation plots (*top*, Fig. 13). The $m = 3$ component in the simulation with the 1.5×10^{-3} pc cluster was more coherent and strong than that with the 1.5×10^{-2} pc cluster (*middle*, Fig. 13). For both simulations, the $m = 4$ components were complicated and varied throughout the disk (*bottom*, Fig. 13).

In Paper I, Pickett et al. discovered that the growth times, radial ranges, and pattern periods of the m-value components of the disturbance did not change much for the different simulations. The main change occurred in the saturation level of the m-values and the duration for which they persisted at that level. For all cases of Paper I, the $m = 2$ grew in 2.4-3.5 MIRPs with a pattern period ~3.5 MIRPs and stayed at the saturation level for the remainder of the simulations. However, the saturation level decreased as the thermal energetics became more realistic, from A_2 ~100% in the ISO case to about A_2 ~10% in the ADI + AV case. In the ISO case, $m = 3$-4 saturated at ~10% and ~30% respectively and persisted at the same level, but in the ADI + AV case, $m = 3$-4 reached only the ~10% and very quickly died to linear levels (~1% or less).

In this study, the growth times and pattern periods did not change significantly between the simulation with the 1.5×10^{-2} pc cluster and that with the 1.5×10^{-3} pc cluster. The radial range for $m = 2$-3 for the simulation with the 1.5×10^{-3} pc cluster was smaller than that with the 1.5×10^{-2} pc cluster. This suggests that in the former simulation, the disk had a more complicated evolution, probably due to the greater gravitational perturbation of the smaller cluster radius. The $m = 2$-4 components of the disturbance in the simulations with the 1.5×10^{-2} pc and 1.5×10^{-3} pc clusters saturated at approximately the same level and persisted there for the duration of the simulations. The $m = 2$ component saturated at a slightly greater level in the simulations with the star clusters than in the ADI + AV case but still much less than the level in the ISO case.

The most remarkable difference between the simulations with a star cluster and the isolated models of Paper I was the significant reduction in τ_2, though the radial range remained approximately the same; the $m = 2$ component of the disturbance grew about three times faster under the influence of the gravitational environment. The different resolutions of the computational grid cannot account for such a large difference. In Paper I, Pickett et al. tested the effect of resolution on the ISO case by running a simulation with resolution (128, 128, 16) and measured τ_2 to be 2.2 MIRPs. As presented in Table 1, with resolution (128, 64, 16), τ_2 was 2.4 MIRPs. More likely, because the disk model proved susceptible to a dominant $m = 2$ disturbance in previous simulations, the gravitational perturbation due to the star cluster merely quickened its growth.

The gravitational perturbation did not dramatically change the evolution of the surface density (Fig. 14). For the simulation with the 1.5×10^{-3} pc cluster, more mass moved inwards from the initial star-disk boundary at 0.15 R_{eq} than in the simulation with the 1.5×10^{-2} pc cluster. Otherwise, the evolution remained approximately the same throughout the rest of the simulation and resembled the evolution of the ADI + AV case.

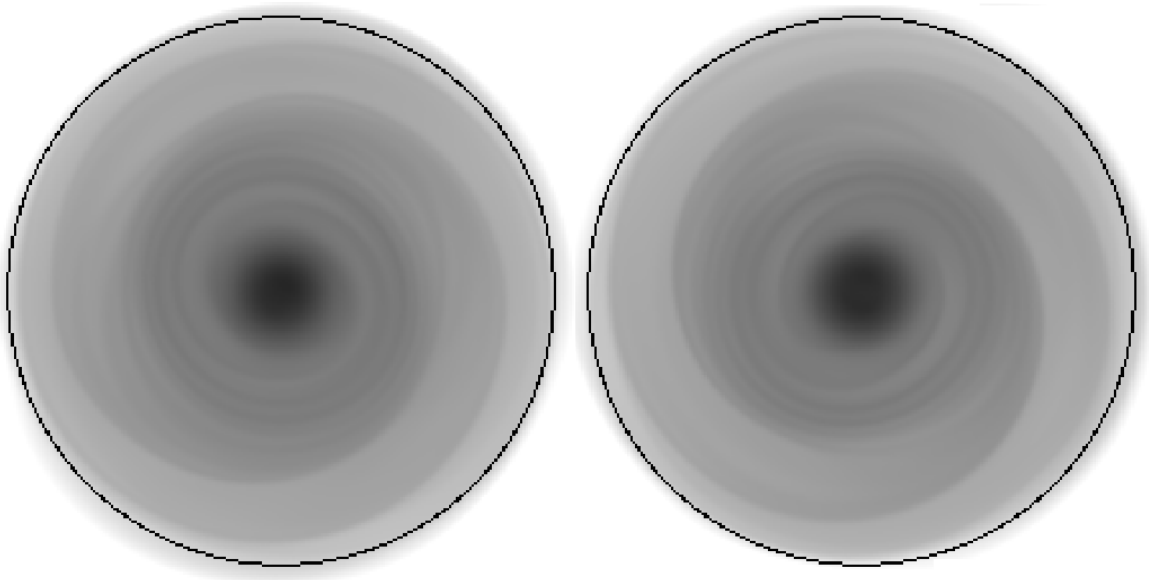

Figure 12: The final equatorial density plots for the simulations with the 1.5×10^{-2} pc (*left*) and 1.5×10^{-3} pc clusters (*right*) at 33.02 MIRPs show more nonaxisymmetric structure than the final image of the ADI + AV case (Fig. 7). The $m = 2$ component dominated the disturbance in both grayscales, but the structure was more coherent and strong in the simulation with the 1.5×10^{-3} pc cluster. The dark outline indicates the initial size of the protostellar disk model. In both simulations, the model has expanded due to internal heating. Some mass has been lost radially, but most mass loss occurs vertically. The star-disk boundary is at about 0.15 R_{eq}. The scale is black for $\rho = 0.3$ and white for $\rho = 3 \times 10^{-7}$, and the sense of rotation is counter-clockwise.

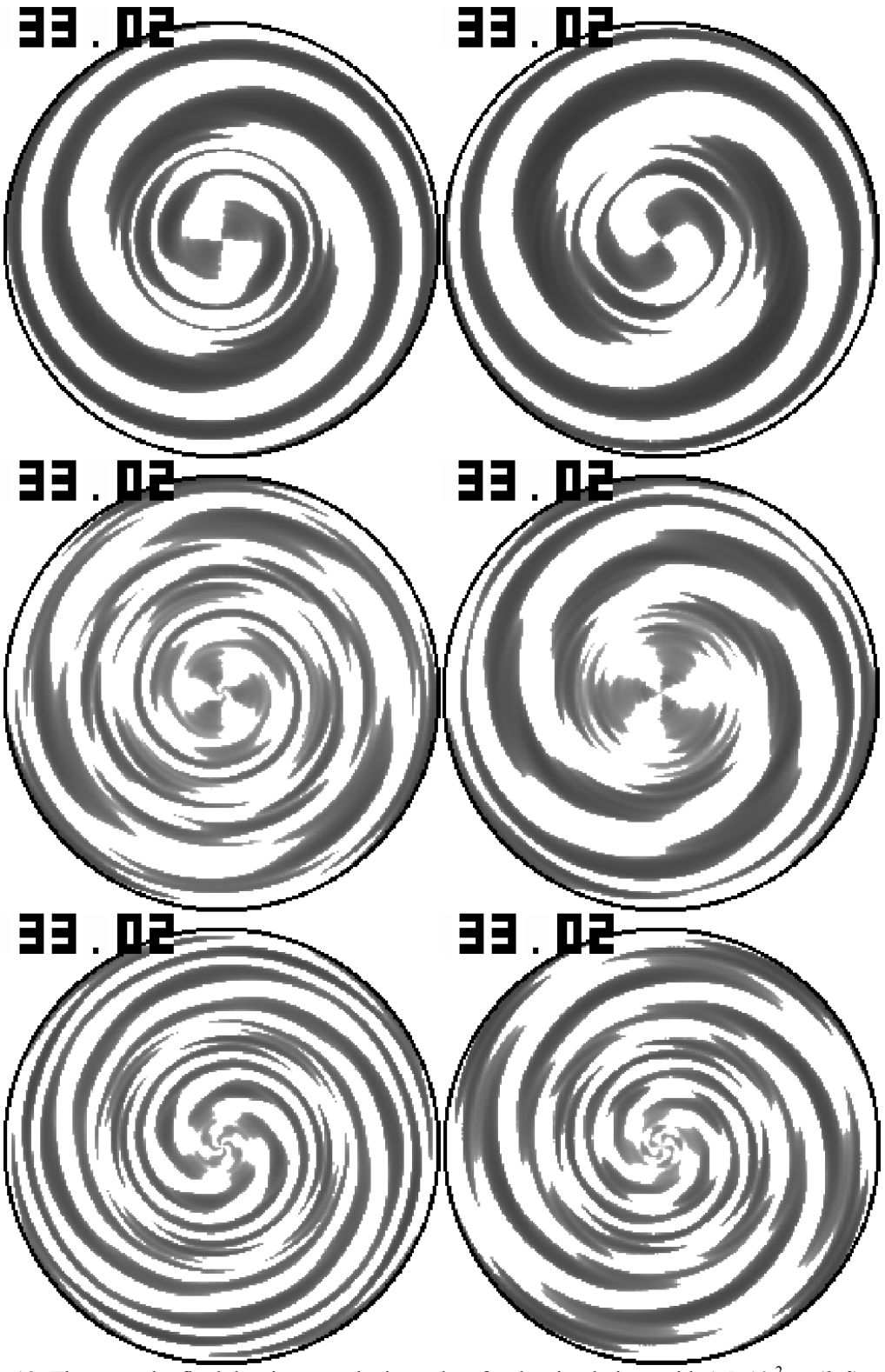

Figure 13: These are the final density perturbations plots for the simulations with 1.5×10^{-2} pc (*left*) and 1.5×10^{-3} pc clusters (*right*) for $m = 2$ (*top*), 3 (*middle*), and 4 (*bottom*) at 33.02 MIRPs. The simulation with the 1.5×10^{-3} pc cluster developed more coherent and strong $m = 2$-3 components. The $m = 4$ components for both simulations show very complicated and varied structure throughout the disk. The scale is black for $\log(A_m) = 0$ and white for $\log(A_m) = -5$, and the sense of rotation is counter-clockwise.

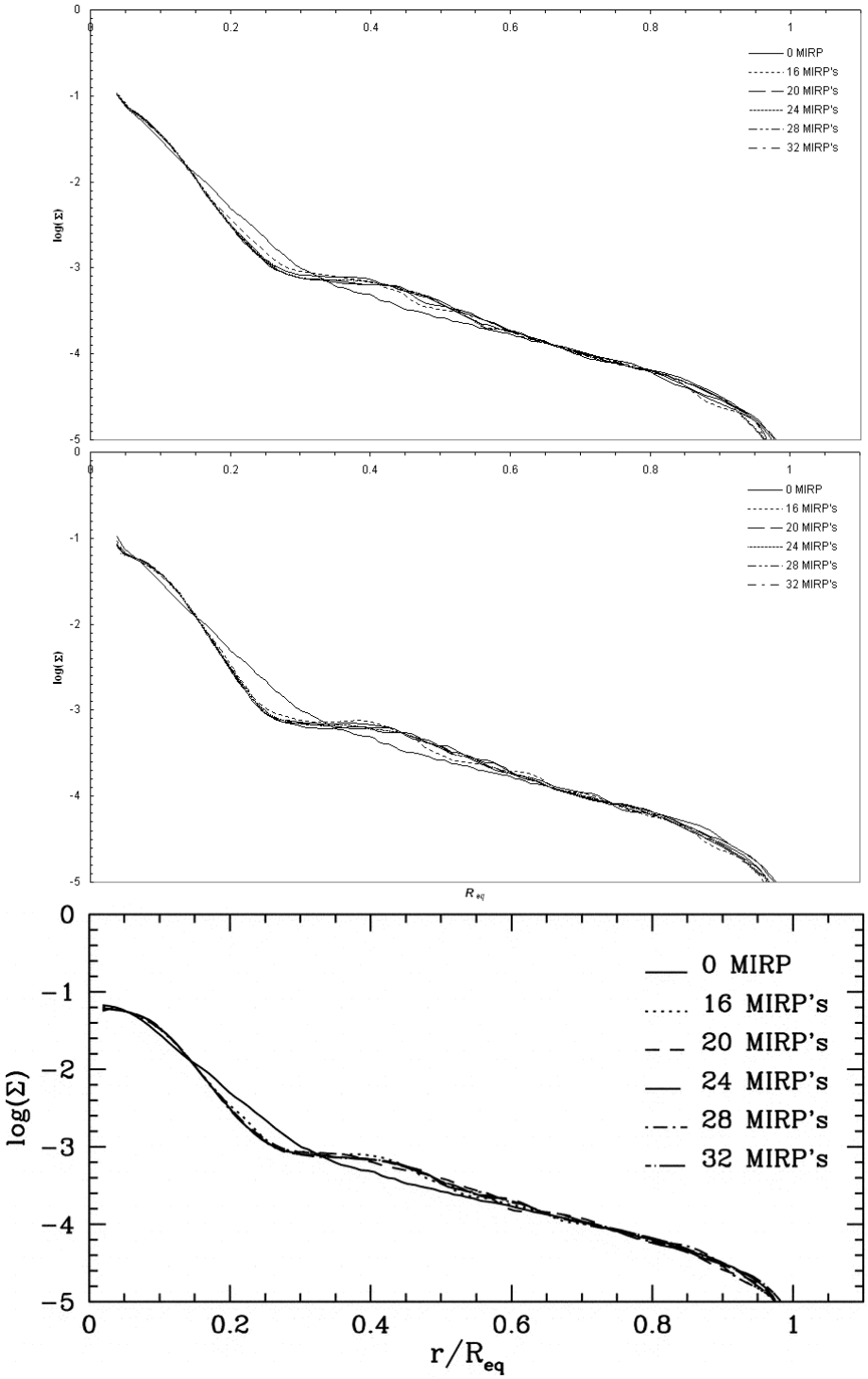

Figure 14: There was no significant change in the evolution of the surface density Σ of the disk in the simulations with 1.5×10^{-2} pc (*top*) and 1.5×10^{-3} pc clusters (*middle*) and the ADI + AV case (*bottom*; Fig. 8, Paper I; reproduced from *Astrophysical Journal*). For all cases, the curves followed the same general trend. By 16 MIRPs, some mass around the initial star-disk boundary, at 0.15 R_{eq}, fell inward onto the star and increased its central density. Mass also moved outwards onto the disk and most greatly increased the density between about 0.3-0.6 R_{eq}. This surface density distribution persisted for the duration of all simulations without much change. The movement of mass at the star-disk boundary was greater for the simulation with the 1.5×10^{-3} pc cluster that for that with the 1.5×10^{-2} pc cluster.

3.3. Model Realism

The question of which star cluster radius in relation to the protostellar disk model best represents reality is crucial to determining the importance of the gravitational environment on the formation of substellar companions. The cluster sizes were varied because the protostellar disk model represented a very young and small, in mass and radius, protostellar disk. If the cluster with the smallest radius were the most realistic, the surrounding star cluster would prove very important in the evolution of a protostellar disk. In this simulation, the model moved halfway across the computational grid in less than 7 MIRPs (Fig. 15). This suggests that the protostellar disk would be moving very quickly through a $1.5\text{x}10^{-4}$ pc cluster and would likely pass very closely to another object, which might lead to a capture or coalescence. The simulations with the $1.5\text{x}10^{-2}$ pc and $1.5\text{x}10^{-3}$ pc clusters were not very different from each other and barely different from the ADI + AV case of Paper I.

It might initially be suggested that the most realistic cluster size is the $1.5\text{x}10^{-4}$ pc, assuming that the cluster size ought to scale linearly as the protostellar disk size. If r_{DISK} were the radius of the model disk, r_{OBS} the radius of observed protostellar disks, and R_{OBS} the radius of observed star clusters, then the magnitude of the appropriate radius for the model cluster, R_{CLUST}, would be as follows:

$$R_{CLUST} = \left(\frac{r_{DISK}}{r_{OBS}} \right) R_{OBS} = \left(\frac{10^{-1}\,AU}{10 - 10^{3}\,AU} \right) 10^{-1}\,pc = 10^{-3} - 10^{-5}\,pc\,. \qquad (5)$$

If this scaling were correct, it would lend credibility to the $1.5\text{x}10^{-4}$ pc cluster as an appropriate size with respect to the protostellar disk model. Therefore, the perturbation due to the gravitational environment would not be negligible in the evolution of a protostellar disk.

However, a better estimation would be to consider the magnitude of the gravitational potential Φ_G, the gravitational force F_G, and the differential tidal force dF_G on the protostellar disk by a cluster member M located at a cluster radius R from the disk of mass m_d and radius dr:

$$\Phi_G = \frac{m_d M}{R}\,; \qquad (6)$$

$$F_G = \frac{m_d M}{R^2}\,; \qquad (7)$$

$$dF_G = \frac{m_d M}{R^3}\,dr\,. \qquad (8)$$

For a 1 M_{SUN} object at the observed cluster radius, $\sim 10^{-1}$ pc, from a typical 1 M_{SUN} disk with radius $\sim 10\text{-}10^3$ AU, Φ_G is on the order of 10, F_G is about 10^2, and dF_G ranges between $10^4\text{-}10^7$. For the simulations presented in this paper, with a 1 M_{SUN} object at the model cluster radii ranging $10^{-2}\text{-}10^{-4}$ pc from the model disk of mass $\sim 10^{-1}$ M_{SUN} and radius 10^{-1} AU, Φ_G, F_G, and dF_G would be as follows: 10, 10^3, and 10^5 for a 10^{-2} pc cluster; 10^2, 10^5, and 10^8 for a 10^{-3} pc cluster; and 10^3, 10^7, and 10^{11} for a 10^{-4} pc cluster. Comparing these values with those for an observed cluster, the $1.5\text{x}10^{-2}$ pc cluster arises as the most realistic size.

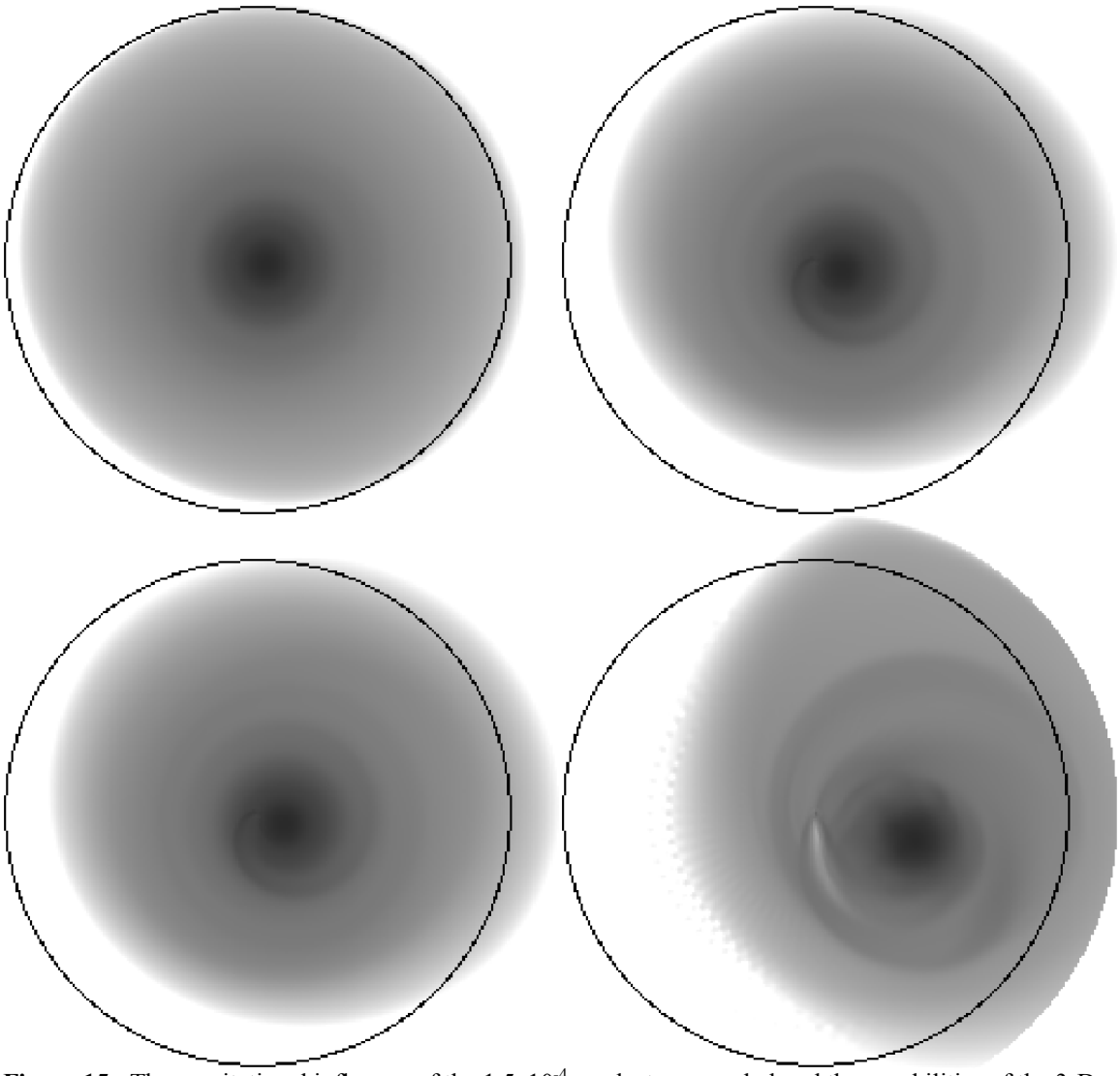

Figure 15: The gravitational influence of the 1.5×10^{-4} pc cluster overwhelmed the capabilities of the 3-D hydrodynamics code and rapidly pulled the protostellar model from the computational grid. These equatorial density plots are for the following times: $t = 1.69$ MIRPs (*top left*), $t = 3.13$ MIRPs (*top right*), $t = 4.53$ MIRPs (*bottom left*), $t = 6.29$ MIRPs (*bottom right*). The black outline indicates the original size and position of the protostellar disk model. The spiral feature seen in the last three images are not physical but artifacts of different portions of the disk sweeping through the center of the computational grid. Similarly, the fringing effect on the left side of the $t = 6.29$ MIRPs is the result of the grid resolution. The scale is black for $\rho = 0.3$ and white for $\rho = 3 \times 10^{-7}$, and the sense of rotation is counter-clockwise.

4. SUMMARY and CONCLUSION

The current study more realistically modeled the formation of substellar companions due to protostellar disk instabilities by including the gravitational influence of the stellar environment. In Paper I, Pickett et al. determined that the internal energetics, namely compressional heating at shock fronts from material moving azimuthally, stabilized a gravitationally isolated disk model known to be subject to an $m = 2$ mode under more stringent thermal conditions, such as the ISO case. When the same young, small in mass and radius disk model evolved under the gravitational influence of a surrounding star cluster, some nonaxisymmetric structure returned. Several simulations were run with clusters of increasingly smaller radii in order to gauge the strength of the gravitational perturbation. In the extreme limit of a 1.5×10^{-4} pc cluster, which was ~20 times the size of the disk, the gravitational perturbation overwhelmed the capabilities of the computational grid. There was little change between the simulations with 1.5×10^{-2} pc and 1.5×10^{-3} pc clusters; they developed some persistent, nonaxisymmetric structure that was similar to the structure seen in the ISO case of Paper I. However, the simulation with the 1.5×10^{-2} pc cluster, which was the most realistic size with respect to the disk mass and radius, developed neither persistent condensations nor even a strong, coherent mode. This suggests that the gravitational environment does not greatly affect the formation of substellar companions.

Future improvements to the code would include placing the disk model at the bottom of the gravitational potential well due to the star cluster (Fig. 16) and accounting for the effect of radiation from the cluster members. The former modification would most likely prevent the center of mass of the disk from moving from the center of the computational grid. If the simulation with the 1.5×10^{-4} pc cluster were run under this condition, the importance of the gravitational environment could be better discerned, because the strength and coherence of the disturbances could be quantified and compared with the other simulations presented here.

Radiation from cluster members may prove more important in the evolution of a protostellar disk than their gravitational influence. Most likely, the radiation, in the form of ultraviolet photons from even one massive cluster member, would stabilize the disk, much as shock heating in the ADI + AV case did. In fact, photoevaporation would occur, leading to significant mass loss. However, there would also be areas of the disk shielded from the radiation and cooler than the neighboring material. This would presumably increase the chance of condensation and, perhaps, substellar companion formation.

In conclusion, the gravitational effect of the star cluster changed the evolution of a well-studied protostellar disk model that was stable to nonaxisymmetric structure. However, this study concludes that the effects are not very important. There are other physical conditions to be included in the three-dimensional hydrodynamics code that may greatly affect the disk. But since the gravitational perturbation of a star cluster does not hinder the simulations, it should be included in future studies because it increases the realism of the modeling.

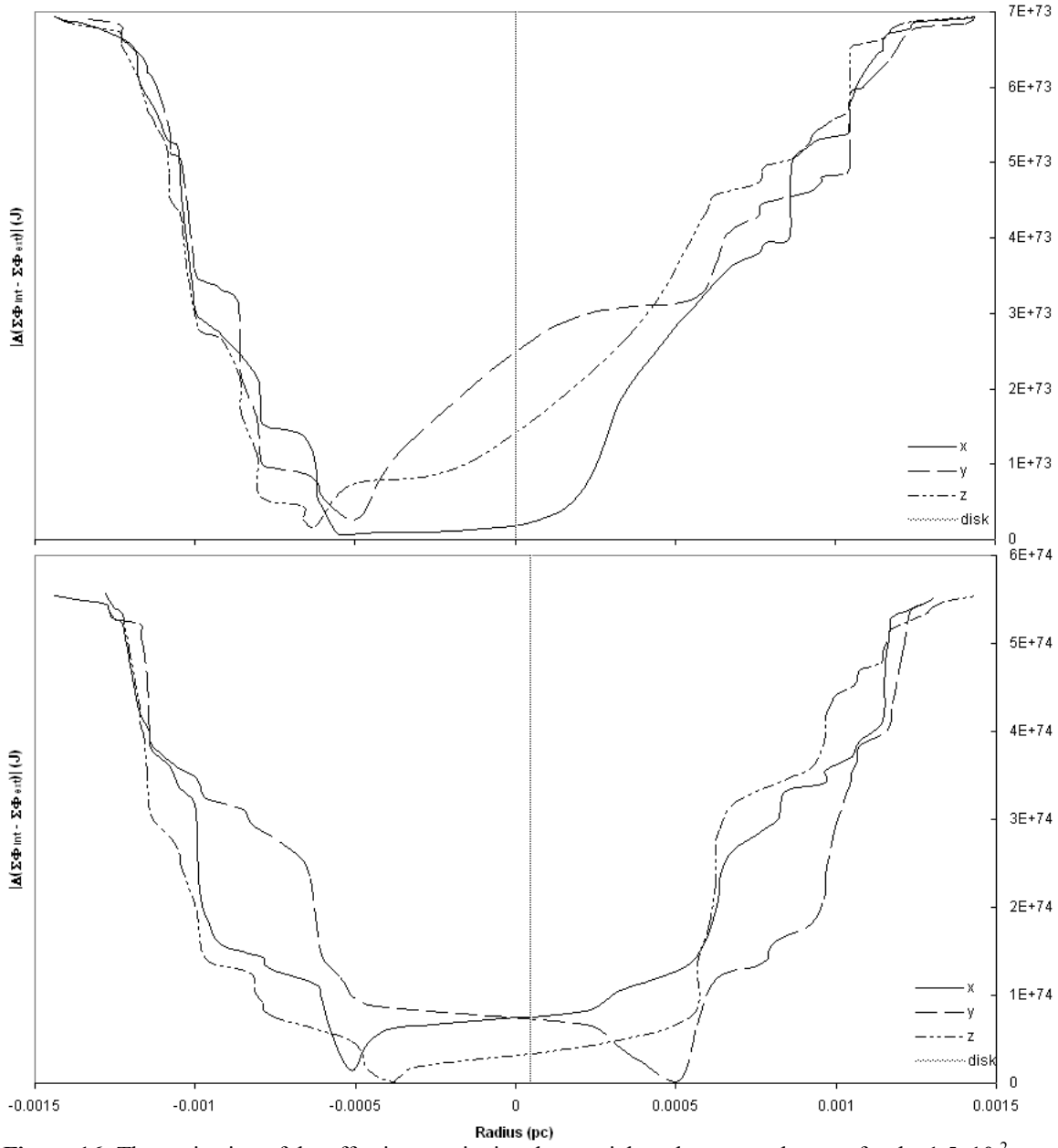

Figure 16: The projection of the effective gravitational potential on the *x*, *y*, and *z* axes for the 1.5×10^{-2} pc (*top*) and 1.5×10^{-3} pc clusters (*bottom*) show the shape of the potential well. For each Cartesian axis, the effective gravitational potential is the absolute difference between $\Sigma\Phi^{-}$, the potential summed from the negative direction, and $\Sigma\Phi^{+}$, the potential summed from the positive direction. Most likely, if the disk were located at the bottom of the well, it would not move significantly from the center of the computational grid. For example, the bottom of the potential well for the simulation with the 1.5×10^{-2} pc cluster was at about -0.5×10^{-2} pc for *x*, *y*, and *z*, while the disk was initially centered at 3×10^{-4} pc, as indicated by the vertical line.

5. REFERENCES

Lada, E. A., Strom, K. M., and Myers, P. C. "Environment of Star Formation: Relationships between Molecular Clouds, Dense Cores and Young Stars." *Protostars and Planets III*. Levy, E. and Lunine, J. I., Eds. 1993: University of Arizona Press

Pickett, B., Cassen, P., Durisen, R., and R. Link. "The Effects of Thermal Energetics on Three-Dimensional Hydrodynamic Instabilities in Massive Protostellar Disks. II. High-Resolution and Adiabatic Evolutions." *Astrophys. J.* 529:1034-1053, 2000 (Paper I)

Pickett, B. "Three Dimensional Hydrodynamics of Protostars and Protostellar Disks." (Dissertation) Indiana University, August 1995

Schneider, J. *The Extrasolar Planets Encyclopedia*. February 1995. <http://cfa-www.harvard.edu/planets/>. 28 April 2003

Tohline, J. E. "The Origin of Binary Stars." *Annu. Rev. Astron. Astrophys*. 40:349-85, 2002

APPENDIX A: STAR CLUSTER CODE

```
      PROGRAM CLUSTER.F

      REAL ::
NOBJ,RCLUST,XCLUST,YCLUST,ZCLUST,MLO,MHI,PSCALE,GSEED
      REAL :: xobj,yobj,zobj,xdif,ydif,zdif,dobj,mobj,prob,mpobj
      CHARACTER :: clustfile*17

      NOBJ=50
      XCLUST=60
      YCLUST=60
      ZCLUST=60
      PSCALE=40
      GSEED=17

C*****Radius of cluster in parsecs*****
      xobj=0.1
C*****Radius of disk in AU*****
      yobj=0.1
      RCLUST=(xobj*3.086d18)/(yobj*1.496d13)/10
C*****Mass of disk in solar masses*****
      mobj=0.5
C*****Min mass of cluster object in solar masses*****
      mpobj=0.2
      MLO=mpobj/mobj
C*****Max mass of cluster object in solar masses*****
      mpobj=10.
      MHI=mpobj/mobj

C*******************************************************
C     Cluster Construction
C     Cluster at (XCLUST,YCLUST,ZCLUST) wrt disk axes
C     RCLUST determines size of cluster
C     MLO and MHI determines range of object masses
C     by Kathy Cooksey, Valparaiso University, 10/2002
C*******************************************************
      clustfile='clust.test'
      open(unit=17,file=clustfile)
 1717 FORMAT(1P5E11.3,1P5E11.3,1P5E11.3,1P5E11.3)
      call srand(GSEED)
      write(17,1717)XCLUST,YCLUST,ZCLUST
      DO i=1,NOBJ
        xobj=XCLUST+(1-2*rand())*RCLUST
        yobj=YCLUST+(1-2*rand())*RCLUST
        zobj=ZCLUST+(1-2*rand())*RCLUST
```

```
  DO
    mobj=rand()*MHI
    prob=rand()*PSCALE
    mpobj=1./sqrt(mobj**3)
    if (prob.lt.mpobj.and.mobj.ge.MLO) exit
  END DO
  write(17,1717)xobj,yobj,zobj,mobj,prob
END DO
STOP
END
```

APPENDIX B: MAIN LOOP OF MODIFIED 3-D HYDRODYNAMICS CODE

```
      Program IU3DHYDRO
C**********************************************************************
C**********************************************************************
C...THIS IS A NEW VERSION OF THE HYDRO CODE WHICH IS SECOND-ORDER IN
BOTH
C...SPACE AND TIME.  S, T ARE FACE-CENTERED; A,RHO,& EPS ARE CELL-
C...CENTERED.   AN ENERGY EQUATION IS INCLUDED FOR ENERGY TRANSPORT.
C...ARTIFICAL VISCOSITY IS USED TO TREAT SHOCKS AND HEAT THE
MODEL.
C...THE FOLLOWING SUBROUTINES ARE CALLED:
C
C     SETUP    :  Read starting models, impose perts, etc.
C     SETMODE  :  Suppress mode m.
C     VLIMIT   :  Limit maximum velocity (usually < 2*SOUND).
C     DELTA    :  Calculate maximum safe delta time.
C     RITE     :  Write output information.
C     SLOPE    :  Calculate van Leer Slope.
C     VLI      :  Calculate van Leer Monotonic Interpolation.
C     FLUX     :  Advect S,T,A,RHO, and EPS.
C     CLEANUP  :  Fix velocities, densities and energy on boundaries.
C     AVISC    :  Artificial Viscosity.
C     SOURCE   :  Source S,T,A, and EPS.
C     VELOCITY :  From momentum densities, calculate velocities.
C     CENTMASS :  Calculate Center of Mass.
C     STATE    :  Equation of State.
C     RAD      :  Radiative Transfer.
C     IMAGE3D  :  Make 3D density imagens.
C     REALTR   :  -|Together These Perform a
C     FFT      :  -|Fast Fourier Transform.
C     POT3     :  Potential Solver.
C     ZAXPHI   :  -|
C     BLKTRI   :  -|
C     BLKTR1   :  -|Various Functions used in/with the
C     PRDCT    :  -|Potential Solvers.
C     COMBP    :  -|
C     TQLRAT   :  -|
C     SETBDY   :  Initialization before BDYGEN.
C     BDYGEN   :  Boundary Potential Solver.
C     SORT     :  Sort.
C     INOUT    :  Load a damped model.
C     DAMP     :  Damp velocities.
C     CLEARUP  :  Clearup after SETMODE or DAMP call.
C     TORQUE   :  Calculate instaneous torques.
C**********************************************************************
```

```
      PARAMETER (jmax=128,JMAX1=JMAX+1,JMAX2=JMAX+2,KMAX=16)
      PARAMETER
(KMAX1=KMAX+1,KMAX2=KMAX+2,LMAX=128,LMAX2=LMAX-2)
C**********Number of cluster objects from cluster.f*********************
      PARAMETER (NOBJ=50)

      COMMON/BLOK6/DTHETA,PI,GRAV

COMMON/BLOK7/RCLOUD,CONSTP,DELT,BDYTEM,DEN,TIME,CORMAS,EPSCEN

COMMON/GRID/JREQ,KZPOL,R(JMAX2),Z(KMAX2),RHF(JMAX2),ZHF(KMAX2),
     &   ROF3N,ZOF3N
      COMMON/AVIS/QRR(JMAX2,KMAX2,LMAX),QZZ(JMAX2,KMAX2,LMAX),
     &         QTT(JMAX2,KMAX2,LMAX),CQ,CS
      REAL JN,mass1,mirp,moneav,totcoefcym(10,8)
      integer jlmmf(0:10)

      common/relimits/rholmt,epslmt,dumlmt
      COMMON/EOM/S(JMAX2,KMAX2,LMAX),T(JMAX2,KMAX2,LMAX),
     &         A(JMAX2,KMAX2,LMAX),
     &         U(JMAX2,KMAX2,LMAX),
     &         W(JMAX2,KMAX2,LMAX),JN(JMAX2,KMAX2,LMAX),
     &         OMEGA(JMAX2,KMAX2,LMAX)

COMMON/STATES/ENON,P(JMAX2,KMAX2,LMAX),CV(JMAX2,KMAX2,LMAX),
     &         EPS(JMAX2,KMAX2,LMAX)
      COMMON/LIMIT/SOUND,vlocal(jmax2,kmax2,lmax)
c      real epsjr,rhojr,ommax
      integer jreq
      COMMON/MISC/EPSJR,RHOJR,OMMAX
      COMMON/POIS/PHI(JMAX2,KMAX2,LMAX),RHO(JMAX2,KMAX2,LMAX)
      COMMON/INSIDE/TMASS,ENEW,ELOST,EDIF,PHICHK,KLOCAT
      COMMON/TIMEST/INDX,ISOADI,ALLOW,DMAX,CHGMAX
      COMMON/COEFS/COEF(JMAX,KMAX2,LMAX2,2)
      COMMON/ITS/ITSTRT,ITSTOP,ITSTEP
      REAL KONST,NPRIME
      COMMON/PTROPE/XN,GAMMA,KONST,NPRIME,TOVERW
      REAL SS(JMAX2,KMAX2,LMAX),TT(JMAX2,KMAX2,LMAX),
     &     AA(JMAX2,KMAX2,LMAX),RRHO(JMAX2,KMAX2,LMAX),
     &     EEPS(JMAX2,KMAX2,LMAX)
      real volume(jmax2),totcoef(8)
      integer timc,m

      real massc(jmax2), massf(jmax2),limmf(10),masst
```

```
      real sumeven(8),sumodd(8),theta(lmax)

C********Cluster Variables, Kathy Cooksey, 2002***************
      REAL :: xobj,yobj,zobj,xdif,ydif,zdif,dobj,mobj
      REAL,DIMENSION(NOBJ,JMAX2,KMAX2,LMAX) :: GRAVPOT
      CHARACTER :: clustfile*17
C*****************************************************

      CHARACTER np*2,tw*3
      CHARACTER tim*6,rhofile*80

      CHARACTER coeffile*17,index*6,modefile*17,centfile*17
      CHARACTER tcoeffile*17,tcoeftenfile*17

      DATA ISTRDN,CHANGD/25,2.00/,NCONS,DELCON/10,2.0/




      TEMPCD=100.0*CHANGD
      MSTORE=IFIX(TEMPCD)
      ITSTEP=0
      MAXTRM=10
      ISYM=2
      ENON=1.d0
      CONSTP=0
      BDYTEM=1.E-3
      CORMAS=1.E-2

c...cq=0 for no AV.  For AV, set CQ=3
c...cs=0 for no shear viscosity (not implemented yet, so don't diddle!)

      CQ=3.D0


      CALL SETUP(ITSTRT,ITSTOP,IDIAG,ISOADI,ISTOR,ITYPE,ITSTEP,ISYM,
     &           MAXTRM)
      write(index,'(i6.6)')itstop

c...setup volumes and angles

      do j=2,jmax1
        volume(j)=0.5d0*dtheta*zof3n*(r(j+1)**2.-r(j)**2.)
      end do
      do l=1,lmax
```

```
        THETA(L)=DTHETA*(L-1)
      END DO


C*******************************************************
C     Cluster Gravitational Perturbation
C     Cluster generated by cluster.f
C     by Kathy Cooksey, Valparaiso University, 10/2002
C*******************************************************
      clustfile='clust.000000'

 1717 FORMAT(1P5E11.3,1P5E11.3,1P5E11.3,1P5E11.3)
      open(unit=17,file=clustfile)

      DO I=1,NOBJ
        read(17,1717)xobj,yobj,zobj,mobj
        print*,xobj,yobj,zobj,mobj
        DO J=2,JMAX2
          DO K=2,KMAX2
            DO L=1,LMAX
              xdif=xobj-RHF(J)*cos(THETA(L))
              ydif=yobj-RHF(J)*sin(THETA(L))
              zdif=zobj-ZHF(K)
              dobj=sqrt(xdif**2+ydif**2+zdif**2)
              GRAVPOT(I,J,K,L)=-mobj/dobj
            END DO
          END DO
        END DO
      END DO
C*******************************************************


      coeffile='coefs.avon.'//index
      modefile='modes.avon.'//index
      centfile='c_o_m.avon.'//index
      tcoeffile='tcoef.avon.'//index
      tcoeftenfile='tctot.avon.'//index

      OPEN(unit=9,file=coeffile)
      OPEN(unit=18,file=modefile)
      OPEN(unit=19,file=centfile)
      open(unit=13,file=tcoeffile)
      open(unit=15,file=tcoeftenfile)
```

```
      CALL RITE(3,-1,1,1,1,1,1,1,1,1,1)
      CALL CLEARUP
      CALL RAD(ISOADI)
      DMAX=0.9*DEN
      CHGMAX=0.0001
      MIRP=2.d0*pi/ommax


      DO 90 ITSTEP=ITSTRT,ITSTOP


        INDX=ITSTEP-ITSTRT


        IHEAD=0
        IF(MOD(INDX,IDIAG).EQ.0) IHEAD=-1
        IPRINT=0
        IF(MOD(INDX,IDIAG).EQ.0) IPRINT=1
        IYES=0
        IF(MOD(INDX,200).EQ.0) IYES=1
        CALL DELTA(IYES)
        TIME=TIME+DELT

C.............................................C
C.....START SECOND ORDER TIME INTEGRATION.....C
C.............................................C

C..(1) 1/2 SOURCE S, T, A, RHO, EPS.

        DELT=DELT/2.0
        CALL SOURCE
        CALL VELOCITY
        CALL VLIMIT


C..(2) STORE QUANTITIES.

        DO 10 K=1,KMAX2
        DO 10 J=1,JMAX2
        DO 10 L=1,LMAX
          SS(J,K,L)=S(J,K,L)
          TT(J,K,L)=T(J,K,L)
          AA(J,K,L)=A(J,K,L)
          RRHO(J,K,L)=RHO(J,K,L)
          EEPS(J,K,L)=EPS(J,K,L)
10      CONTINUE
```

```
C..(3) 1/2 FLUX S, T, A, RHO, EPS.

      CALL FLUX(S,T,A,RHO,EPS)
      CALL VELOCITY
      CALL VLIMIT



C..(4) 1 FLUX SS, TT, AA, RRHO, EEPS,
C.......BUT USE S, T, A, RHO, EEPS TO CALCULATE FLUXES.

      DELT=2.0*DELT
      CALL FLUX(SS,TT,AA,RRHO,EEPS)


C..(5) UPDATE S, T, A, RHO, EPS.

      DO 20 K=1,KMAX2
      DO 20 J=1,JMAX2
      DO 20 L=1,LMAX
        S(J,K,L)=SS(J,K,L)
        T(J,K,L)=TT(J,K,L)
        A(J,K,L)=AA(J,K,L)
        RHO(J,K,L)=RRHO(J,K,L)
        EPS(J,K,L)=EEPS(J,K,L)

 20     CONTINUE



C..(6) 1/2 SOURCE S, T, A, RHO, EPS.


      CALL VELOCITY
      CALL VLIMIT
      CALL CLEARUP

      CALL RAD(ISOADI)


      REDGE=R(JMAX1)
      CALL BDYGEN(MAXTRM,ISYM,REDGE)
      CALL POT3(8,IPRINT)

C********Gravitational Perturbation, Kathy Cooksey, 2002*********
```

```
      DO I=1,NOBJ
        DO J=2,JMAX2
          DO K=2,KMAX2
            DO L=1,LMAX
              PHI(J,K,L)=PHI(J,K,L)+GRAVPOT(I,J,K,L)
            END DO
          END DO
        END DO
      END DO

c       DO J=2,JMAX
c         print*,J,GRAVPOT(1,J,2,1)
c       END DO
C*********************************************************

      DELT=DELT/2.0
      CALL STATE
      CALL SOURCE



C..(7) UPDATES DUE TO ENERGY EQUATION

      CALL STATE


      CALL VELOCITY
      CALL VLIMIT
      CALL CLEARUP
      DELT=2.*DELT



C.............................................C
C.....COMPLETED ONE TIME STEP INTEGRATION.....C
C.............................................C
```

APPENDIX C: UNITS

There are several units of time, mass, and length applicable to the simulations of the 3-D hydrodynamics code. Central initial rotation period (CIRP) and minimum initial rotation period (MIRP) are best used for simulations of protostars and protostellar disks, respectively, in order to relate the time essentially to the number of rotations the object has undergone. Polytropic units (PU) are the dimensionless code units of time, mass, and length for any simulation when the model mass, the gravitational constant, and the time-independent constant of pressure (i.e., the polytropic constant) are set equal to unity. In this manner, the polytropic unit of time, mass, or length corresponds to the physical property of the model. The pertinent quantities of the protostellar disk model studied in this paper are as follows:

45 PU (time) = 1 MIRP
1 PU (mass) = 0.5 M_{SUN}
1 PU (length) = 0.1 AU. (C.1)

Another useful unit of length is the initial equatorial radius, R_{eq}, of the protostellar disk model, which is not necessarily the radial size of the computational grid. For the model studied here, R_{eq} is at $j = 107$, and the grid is (128, 128, 16) in (r, φ, z). The star-disk boundary is at $j = 16$ or 0.15 R_{eq}.

It was occasionally necessary to scale the minimum initial rotation period when using the analysis programs of Paper I (see § 3.1). This was accomplished by basically defining MIRP', as follows:

MIRP' = $^7/_4$ MIRP = 78.75 PU (time). (C.2)

In Figures 8 and 9, the horizontal axis is actually in units of MIRP'. The growth times and errors indicated in Figure 9 are in units of MIRP'. These values were scaled by 7/4 to convert them to units of MIRP:

$[\tau_m]$ = MIRP' = $^7/_4$ MIRP. (C.3)

These scaled growth times and errors were quoted in Table 1.